REPORT DOCUMENTATION PAGE

Form Approved
OMB No. 0704-0188

1. AGENCY USE ONLY (Leave blank)	2. REPORT DATE	3. REPORT TYPE AND DATES COVERED
	February 1994	

4. TITLE AND SUBTITLE
Multiple-Channel Equalization of a Nearfield Sonar System

5. FUNDING NUMBERS
N00039-92-C-0100

6. AUTHOR(S)
S. J. Barnett

7. PERFORMING ORGANIZATION NAME(S) AND ADDRESS(ES)
Applied Research Laboratory
The Pennsylvania State University
P.O. Box 30
State College, PA 16804

8. PERFORMING ORGANIZATION REPORT NUMBER
TR#94-06

9. SPONSORING / MONITORING AGENCY NAME(S) AND ADDRESS(ES)
Naval Undersea Warfare Center Division
Keyport, WA 98345-0580

10. SPONSORING / MONITORING AGENCY REPORT NUMBER

11. SUPPLEMENTARY NOTES

12a. DISTRIBUTION / AVAILABILITY STATEMENT
Unlimited

12b. DISTRIBUTION CODE

13. ABSTRACT *(Maximum 200 words)*

Adaptive equalization, although most commonly applied in communications, is necessary in many instances where signal fidelity must be maintained throughout a channel's medium. Adaptive equalization technology was used here as a solution to the problem of equalization a multiple-channel nearfield sonar system. Before compensation, a subset of the channels is characterized to assess the magnitude of the problem and the margin for performance improvement. This characterization data provides evidence that equalization is absolutely essential if the sonar system is to perform with any degree of accuracy. After a brief description of the selected processor, equalization is performed on the selected channels. Channel characterization data from before and after compensation is then compared to examine performance enhancements.

14. SUBJECT TERMS
multiple channel equalization, nearfield, sonar

15. NUMBER OF PAGES
77

16. PRICE CODE

17. SECURITY CLASSIFICATION OF REPORT	18. SECURITY CLASSIFICATION OF THIS PAGE	19. SECURITY CLASSIFICATION OF ABSTRACT	20. LIMITATION OF ABSTRACT
UNCLASSIFIED	UNCLASSIFIED	UNCLASSIFIED	UNLIMITED

Applied Research Laboratory

Technical Report

PENNSTATE

1855

The Pennsylvania State University
APPLIED RESEARCH LABORATORY
P.O. Box 30
State College, PA 16804

MULTIPLE-CHANNEL EQUALIZATION OF A NEARFIELD SONAR SYSTEM

by

S. J. Barnett

Technical Report No. TR 94-06
February 1994

Supported by:
Naval Undersea Warfare Center Division

L.R. Hettche, Director
Applied Research Laboratory

ABSTRACT

Adaptive equalization, although most commonly applied in communications, is necessary in many instances where signal fidelity must be maintained throughout a channels's medium. Adaptive equalization technology was used here as a solution to the problem of equalizing a multiple-channel nearfield sonar system. Before compensation, a subset of the channels is characterized to assess the magnitude of the problem and the margin for performance improvement. This characterization data provides evidence that equalization is absolutely essential if the sonar system is to perform with any degree of accuracy. After a brief description of the selected processor, equalization is performed on the selected channels. Channel characterization data from before and after compensation is then compared to examine performance enhancements.

TABLE OF CONTENTS

LIST OF FIGURES

LIST OF TABLES

Chapter 1

INTRODUCTION

Equalizers are used in a wide variety of applications where signal distortion must be eliminated. The distortion is caused by the propagation medium's transfer function having a non-uniform amplitude or non-linear phase versus frequency response at frequencies where there is significant energy in the signal. In order to overcome these phenomena, it is necessary to insert a transfer function in series with the medium's transfer function that is its inverse, thus achieving equalization.

Equalizers are often implemented as fixed networks. Usually, a filter is inserted in series with the signal path in order to get the desired result. However, if a multiple-channel system needs to be equalized, the filter alignment required for all channels can become quite tedious, and realignment may be periodically necessary due to changes in the environment. In these cases, an adaptive equalizer becomes more desirable than its fixed counterpart. It can automatically synthesize the medium's inverse transfer function when given appropriate reference signals and training periods.

Extensive research has been conducted on the application of adaptive equalizers with communications channels, specifically in channels corrupted by InterSymbol Interference (ISI) [1, 2, 4, 6, 10]. In this case, the system could have multiple channels and possibly have transfer functions that drift with time. Here, adaptive equalization is preferred over its fixed-network counterpart due to repetitive filter alignment and calibration issues. A block diagram of a typical communications channel is illustrated in Figure 1.

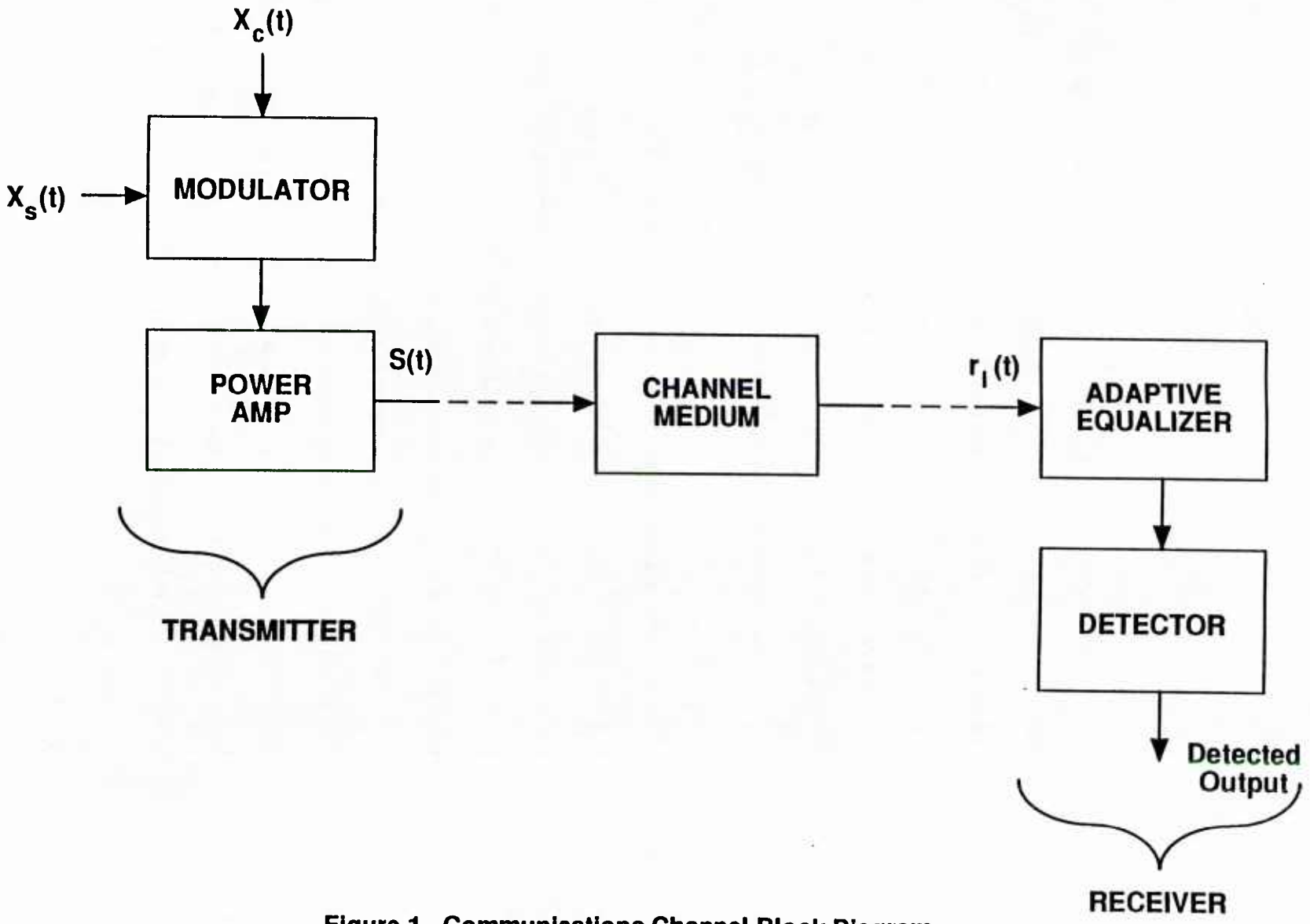

Figure 1. Communications Channel Block Diagram

The inputs to the modulator are the baseband information signal $X_s(t)$ and the carrier signal $X_c(t)$. A modulated and amplified carrier output s(t) is then input to the channel. The signal is distorted in amplitude and phase as it propagates through the channel. Both of these linear types of distortion contribute to time dispersion or pulse lengthening. At the receiver, where the signal is demodulated and detected, problems occur if there is significant time dispersion. Symbol energy in one time slot at the transmitter but dispersing into adjacent time slots at the receiver results in symbol detection errors and therefore the channel's performance is degraded considerably. However, the adaptive equalizer helps overcome this problem.

In practice, a test signal with its energy contained in the passband of interest is transmitted through the channel. The received signal is operated on by the equalizer and then compared to a reference signal. The difference or error signal is used to update the equalizer weights. Once the weights have been calculated, normal operation may follow with the equalizer and its optimum set of weights in place. This automatic adjustment of the weights inherent in adaptive equalizers allows compensation for channel characteristics unknown a priori. On the other hand, fixed network equalizers require knowledge of channel characteristics before the weights are adjusted. Their weights compensate for an average range of linear distortion. This may provide inadequate performance in multiple-channel systems with a large variance in channel characteristics. In addition, the amount of work required to generate tap settings for each channel would be prohibitive. Therefore, the automatic synthesis of weight settings performed by adaptive equalizers is a much more efficient means of channel equalization for multi-channel systems.

Assuming the diagram in Figure 1 represents a discreet communications system, then $x_s(t)$ becomes a sequence representing the symbol to be transmitted during each time slot. If each element of the sequence is denoted by x_n, then the output of the modulator, after power amplification, is given by

$$s(t) = \sum_{n=0}^{\infty} x_n x_c(t-nT) \tag{1}$$

where $x_c(t)$ is the pulsed carrier signal and x_n is an element of the sequence whose value is dependent upon the type of modulation, i.e. Pulse Amplitude Modulation (PAM), Phase Shift Keying (PSK), Frequency Shift Keying (FSK), etc. The value "T" represents the transmission time, with one symbol being transmitted every T seconds. If it is assumed that the channel's impulse response is g(t), then the input to the receiver is

$$r_i(t) = \int_{-\infty}^{\infty} g(\tau)\, s(t-\tau)\, d\tau \tag{2}$$

Substitution for s(t) in this expression then results in

$$\begin{aligned} r_i(t) &= \int_{-\infty}^{\infty} g(\tau) \left[\sum_{n=0}^{\infty} x_n x_c(t-\tau-nT) \right] d\tau \\ &= \sum_{n=0}^{\infty} x_n \int_{-\infty}^{\infty} g(\tau)\, x_c(t-\tau-nT)\, d\tau \end{aligned} \tag{3}$$

Since the channel's response to the pulsed carrier signal can be represented by

$$h(t) = \int_{-\infty}^{\infty} g(\tau)\, x_c(t-\tau)\, d\tau \tag{4}$$

then the receiver input simplifies to

$$r_i(t) = \sum_{n=0}^{\infty} x_n h(t-nT) \tag{5}$$

So far, there has been no allowance for propagation delay and relative time difference between transmit and receive samples. Denoting these parameters collectively by t_d, if the baseband signal is sampled at the receiving end at instants t = kT seconds for k=0, 1, 2, . . ., the receiver samples (assuming all signals are at baseband) are given by

$$r_s(kT) = r_i(kT+t_d) = \sum_{n=0}^{\infty} x_n h(kT+t_d-nT)$$

or

$$r_s(kT) = x_k h(t_d) + \sum_{\substack{n=0 \\ n \neq k}}^{\infty} x_n h(kT+t_d-nT) \tag{6}$$

for k=0, 1, 2, . . . j. It should be noted that in some derivations an additive noise term is included in the above expression to represent interference injected by the channel medium itself. However, it is omitted here for the sake of clarity. The first term on the right is the desired result, while the summation term is interference from neighboring time slots. Notice that if h(t) possesses significant energy in neighboring time slots, or h(t) >> 0 for $|t| > T/2$, then interference is added to $r_s(kT)$. If it lowers the Signal-to-Noise Ratio (SNR) enough, the detection threshold of the receiver may be compromised, thereby allowing detection errors and a dramatic loss in performance. However, if an equalizer is inserted before the detector, the time dispersion and resulting performance loss can be reduced or eliminated completely. Since there is a wide variety of adaptive equalizers available, several parameters must be considered

when choosing one. Two such parameters are filter type and coefficient optimization algorithms.

There are numerous filter types available for equalization, both recursive and non-recursive [2, 5]. In the non-recursive arena, the transversal and fractionally spaced configurations are widely used for combatting ISI. Of these, the transversal configuration is probably the most commonly used and will be discussed first. Figure 2 is a block diagram of the transversal filter which shows that as each new sample is input, the oldest one is discarded. The remaining samples are then multiplied by their respective tap gain and the results are added to provide the final result. Mathematically, this is represented by the expression

$$y(n) = \sum_{l=0}^{N-1} c_l x_{n-l} \tag{7}$$

where x_{n-l} are the past inputs, c_l are the filter weights for an N-tap filter, i.e. l=0, 1, 2, . . . N-1, and y(n) is the output at time t=nT. From the discrete convolution expression above, the simplicity of this filter architecture becomes obvious.

A similar type of filter is the Fractionally Spaced Equalizer (FSE) [5]. This filter is actually a transversal type with a higher sampling rate, by a factor of two or three, than the usual 1/T rate. At the filter output, the samples are decimated or sampled at the transmission rate. The main benefit of an FSE is its insensitivity to sampler phase relative to the incoming signal at the receiver. An equalizer with 1/T sampling (assuming equalizer input is at baseband) causes aliasing of the input spectrum and then, due to this phase difference, the resulting spectrum near the band edges will have nulls and peaks depending on whether there is constructive or destructive addition of aliased

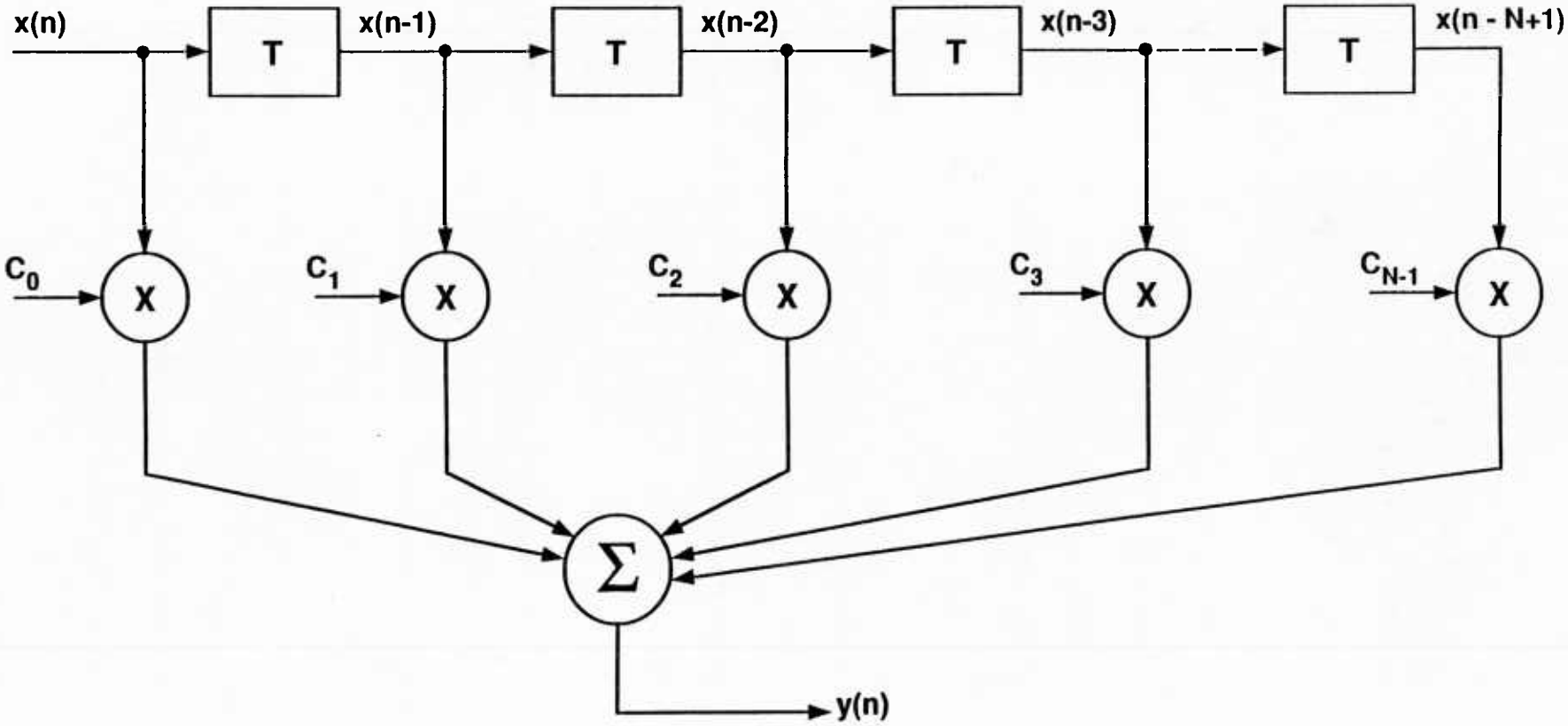

Figure 2. Transversal Filter

components. In addition, this phase may be time-varying, causing the distribution of nulls and peaks in the resultant spectrum to change with time. In effect, it is a very difficult if not impossible task to equalize near the band edges of the pulse spectrum. However, due to its higher sampling rate, an FSE reduces the aliasing problem and provides much better equalization performance near the band edges.

In the recursive filter domain, a common structure is the Decision Feedback Equalizer (DFE). The DFE uses basic transversal filters in feed-forward and feedback sections as shown in Figure 3 [5, 7]. The output z(k) is given by the expression

$$z(k) = \sum_{l=0}^{N-1} C_l x_{k-l} - \sum_{m=1}^{M-1} b_m d_{k-m} \qquad (8)$$

A linear combination of past decisions, assumed to be correct, are fed back via the feedback section. Therefore, any interference produced by these symbols can be subtracted from the feed-forward section. The main advantage of the DFE over its linear transversal counterpart is that it can counteract distortion without adding excessive noise to the communication channel. Since the combined impulse response of the channel and equalizer is a unit impulse for perfect matching, maximum noise power is allowed through the channel to the detector. However, the feedback section of a DFE removes such stringent impulse response requirements from the feed-forward section and thus reduces total noise power input to the detector.

So far, filter architectures have been discussed and much has been said about filter weights but nothing has been mentioned about their settings or adjustments.

In choosing a set of filter weights, the criterion used as the basis for the selection must first be established [8]. The most common criterion used is Mean-Square Error

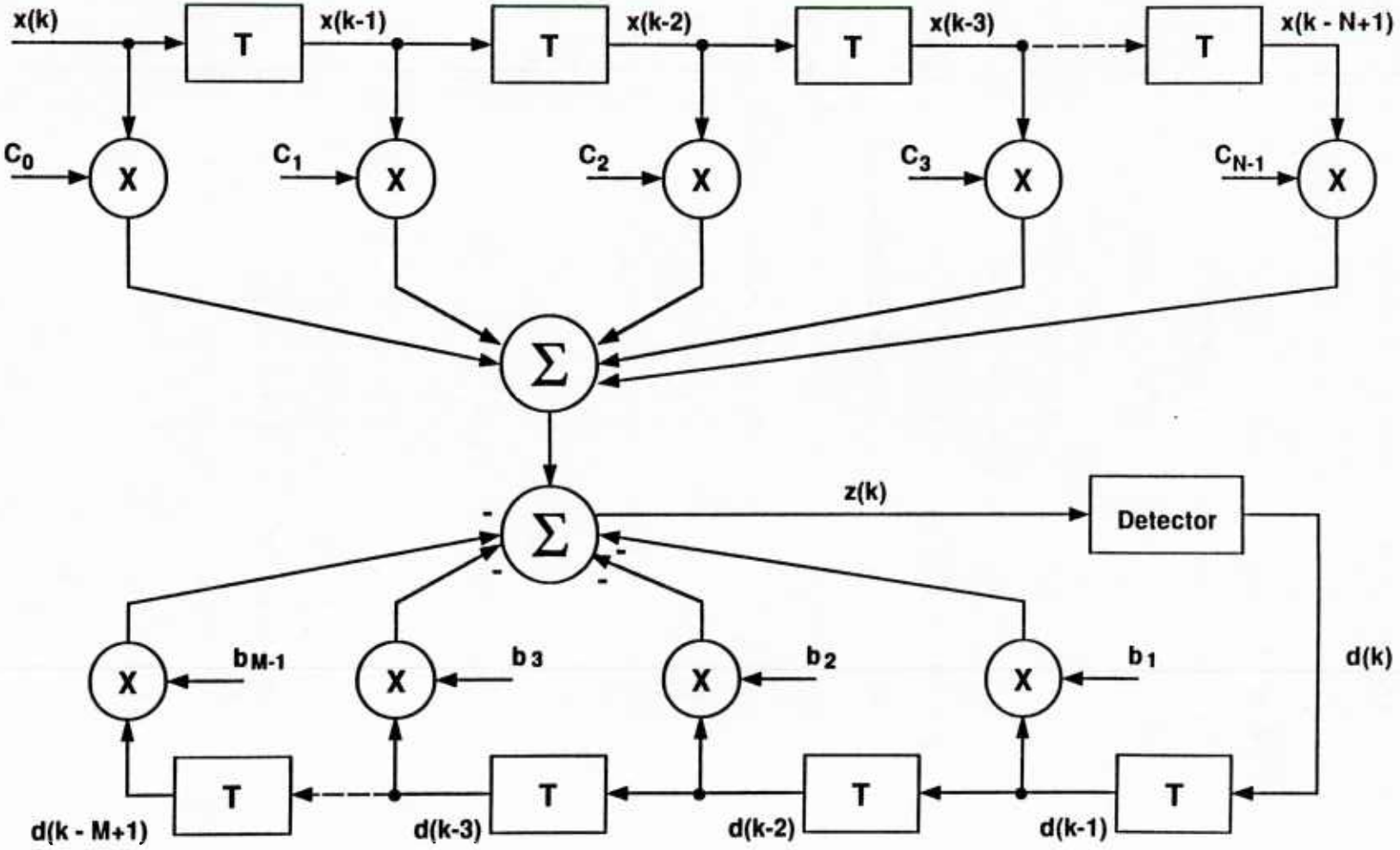

Figure 3. Decision Feedback Equalizer (DFE)

(MSE), whereby taps are chosen such that the mean-square error, or difference, between a reference and equalizer output is minimized. Using this criterion, the optimum weight settings must be calculated using input statistics which are not known a priori. Therefore, an iterative procedure must be used to obtain the desired weights. The expression used to calculate the coefficients is described by

$$\vec{C}_{i+1} = \vec{C}_i + \Delta_i \vec{S}_i \quad ; \; i = 0, 1, 2, \ldots \tag{9}$$

where $\vec{C}_i$ is the vector of coefficients, Δ_i is the step size or loop gain, and $\vec{S}_i$ is the direction vector -- all of which are evaluated at the i^{th} iteration. In practice, Δ_i is usually chosen based on a tradeoff between the speed of convergence and output-noise-power, the latter caused by the coefficients fluctuating about their optimum values. The vector $\vec{S}_i$ is dependent upon the numerical algorithm used, three of which are: 1) steepest descent, 2) conjugate gradient, and 3) Fletcher-Powell [6, 9, 10]. The most popular method, steepest descent, has a direction vector given by

$$\vec{S}_i = -\vec{g}_i \tag{10}$$

where $\boldsymbol{g}_i$ is an N-dimensional vector of gradient components

$$\vec{g}_i = -E[\varepsilon_i \vec{y}_i^*] \tag{11}$$

In this expression, E[ ] is the expectation operator, ε_i is the error between the reference and equalized signals, and $\vec{y}_i$ is the vector of past and present input samples at the i^{th} iteration. However, since the required expectation information is not readily available, an estimate of the form

$$\vec{g}_i = -\varepsilon_i \vec{y}_i^* \tag{12}$$

is used instead. Then, the recursive algorithm becomes

$$\vec{C}_{i+1} = \vec{C}_i + \Delta_i \varepsilon_i \vec{y}_i^* \quad ; \; i = 0, 1, 2, \ldots$$

Once the equalizer is in place but before operation can begin, it must go through a training period to generate the proper tap settings. A signal, which might be a Pseudo-Random-Noise (PRN) sequence for example, is input to the channel. A delayed replica is applied to the reference input of the equalizer while the other input is driven by the output of the channel. After the equalizer has had time to calculate the weights, the coefficient update capability is disabled and the equalizer operates as a FIR filter with the calculated weights. Communication over the channel can now begin with the training cycle completed.

1.1 Statement of the Problem

Thus far, the discussion has revolved around adaptive equalization as it applies to communication channels. In fact, the majority of literature currently available deals with the problem of equalizing communication channels or, more specifically, eliminating InterSymbol Interference (ISI). However, in this research publication, it is of great interest to utilize adaptive techniques in performing multiple-channel equalization of a nearfield sonar system.

The sonar system is capable of producing an acoustic field at a point under water where a Receiver Under Test (RUT) is located. A block diagram of such a system is

shown in Figure 4. The system consists of "n" independent channels driven by inputs that are amplitude-shaded in order to produce sonar signals at the RUT which appear to come from different points in space. Each of the signals, $S_1(k)$. . .$S_n(k)$, is in the digital domain, and they are identical with the exception of amplitude. These signals drive the channels' electronics which consist of Digital-to-Analog (D/A) converters, preamplifiers, filters, power amplifiers, etc. The output signal, consisting of any combination of broadband and narrowband energy, is converted to acoustic energy via the transducer. Broadband refers to energy distributed across most of the 1.6 kHz system bandwidth, while narrowband refers to energy contained in a much smaller sub-band within the same bandwidth. The acoustic energy then propagates to the RUT where it is added to the energy from the other channels. At the RUT, there will be a composite signal consisting of a noise source, an echo and reverberation. In addition, due to amplitude shading of each of the multiple drivers in the projector array, this signal will appear to come from a region under water in some subspace of three-dimensional space.

The amplitude-shaded array's principle of operation requires that a coherent (in-phase) sum must exist at the RUT's location when each element in the array is being driven with in-phase signals. This in turn requires matching acoustic path lengths as well as the driver electronics' signal group delay between channels.

Matching path lengths would be a difficult problem due to the mechanical tolerances of the array's fixture. In addition, matching the electronics between channels would be a tedious and costly venture. However, if channel equalization could be achieved using adaptive filters, it could be performed in a relatively simple and elegant manner. Therefore, the objective of this research is to match amplitude and group delay

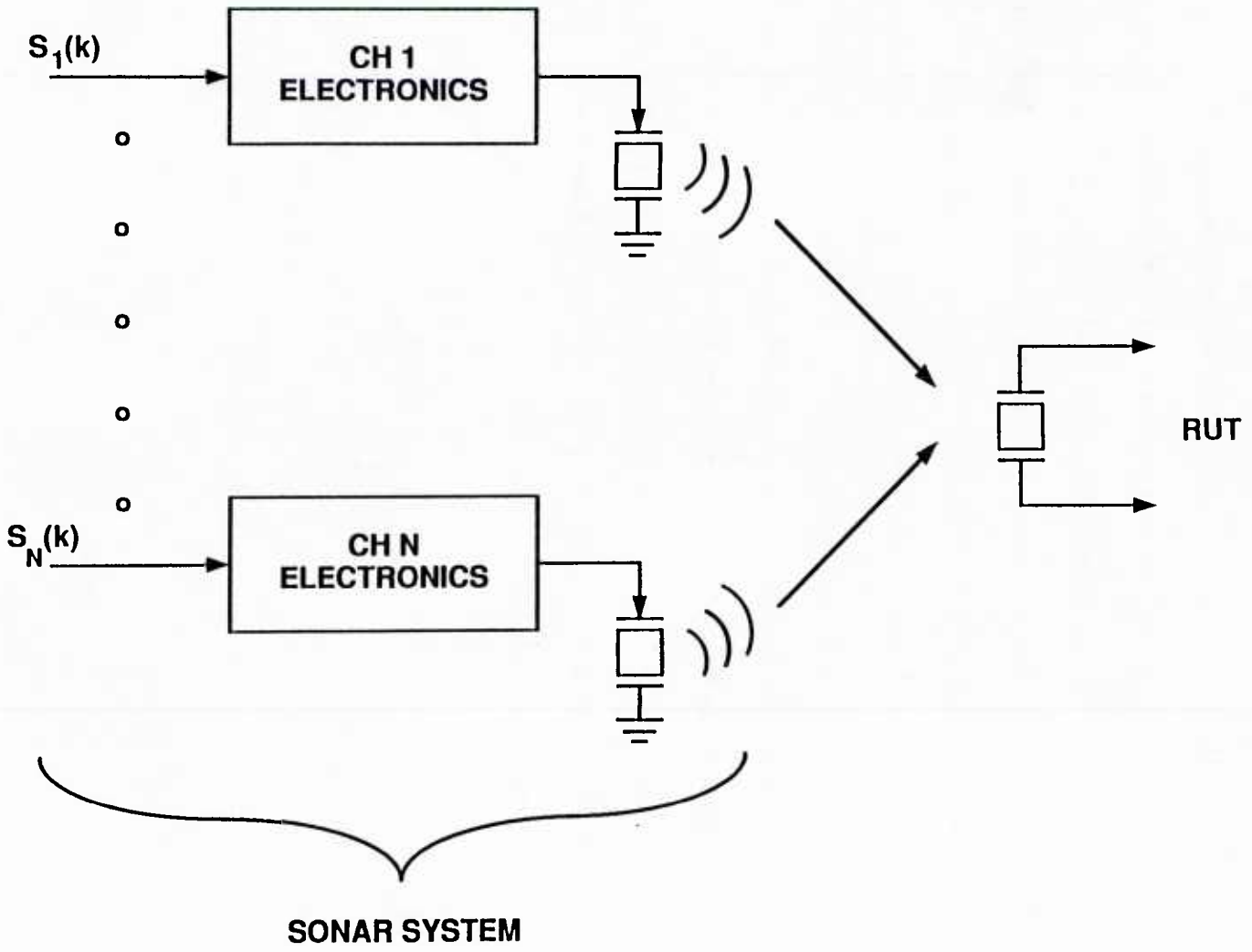

Figure 4. Nearfield Sonar System with Receiver Under Test (RUT)

between channels, from the channel input to the RUT, utilizing an adaptive equalization approach.

In what follows, a proposed solution is given together with qualitative and/or quantitative analysis and modeling where appropriate. Unequalized measurements are then performed in order to characterize each channel's performance and transfer function (the system is assumed to be linear). After choosing the adaptive digital filter and associated parameters, equalization results are examined. Such items as loop gain versus rate of convergence are examined as well as the filter's time and frequency domain responses. The comparison between equalized and unequalized results is probably most important. This gives an indication of how well the equalizer approximates the channel's inverse transfer function and, more importantly, of improvements in overall system performance levels. Finally, this publication will include an overall summary and any conclusions that can be drawn from the research and experimental work.

Chapter 2

PROPOSED SOLUTION

As indicated in Section 1.1, an unequalized nearfield sonar system exists as depicted in Figure 4. The proposed solution is to equalize each of the N channels using adaptive filters. One is inserted in series with each channel's electronics for channels 1 to N. The composite transfer function existing now between $S_x(k)$ and the RUT is

$$H_x(\omega) = F_x(\omega)\, C_x(\omega) \tag{13}$$

where $F_x(\omega)$ and $C_x(\omega)$ are the transfer functions of the adaptive filter and medium of channel x, respectively. It approaches the theoretical limit of

$$H_x(\omega) = e^{-j\omega\tau_d} \tag{14}$$

where τ_d is the total delay through the channel. In order to generate the weights for each filter, a configuration is utilized called the ADAPT mode (see Figure 5). Here, a broadband noise source is used as a reference to excite the channel while a delayed version drives the desired input of the adaptive loop. A conditioned output from the channel closes the loop and enables generation of the weights. Once the weights have been established, the channel enters the RUN mode (see Figure 6) with the weights left in place. Referring to Figures 5 and 6, it is assumed that: 1) the adaptive equalizer operates in the digital domain; 2) the system center frequency, f_o = 12 kHz; 3) the system bandwidth, W = 1.6 kHz; 4) the digital sampling rate, f_s = 9.76 kHz; 5) channel characteristics do not change appreciably while in RUN mode; and 6) there is no convergence rate requirement.

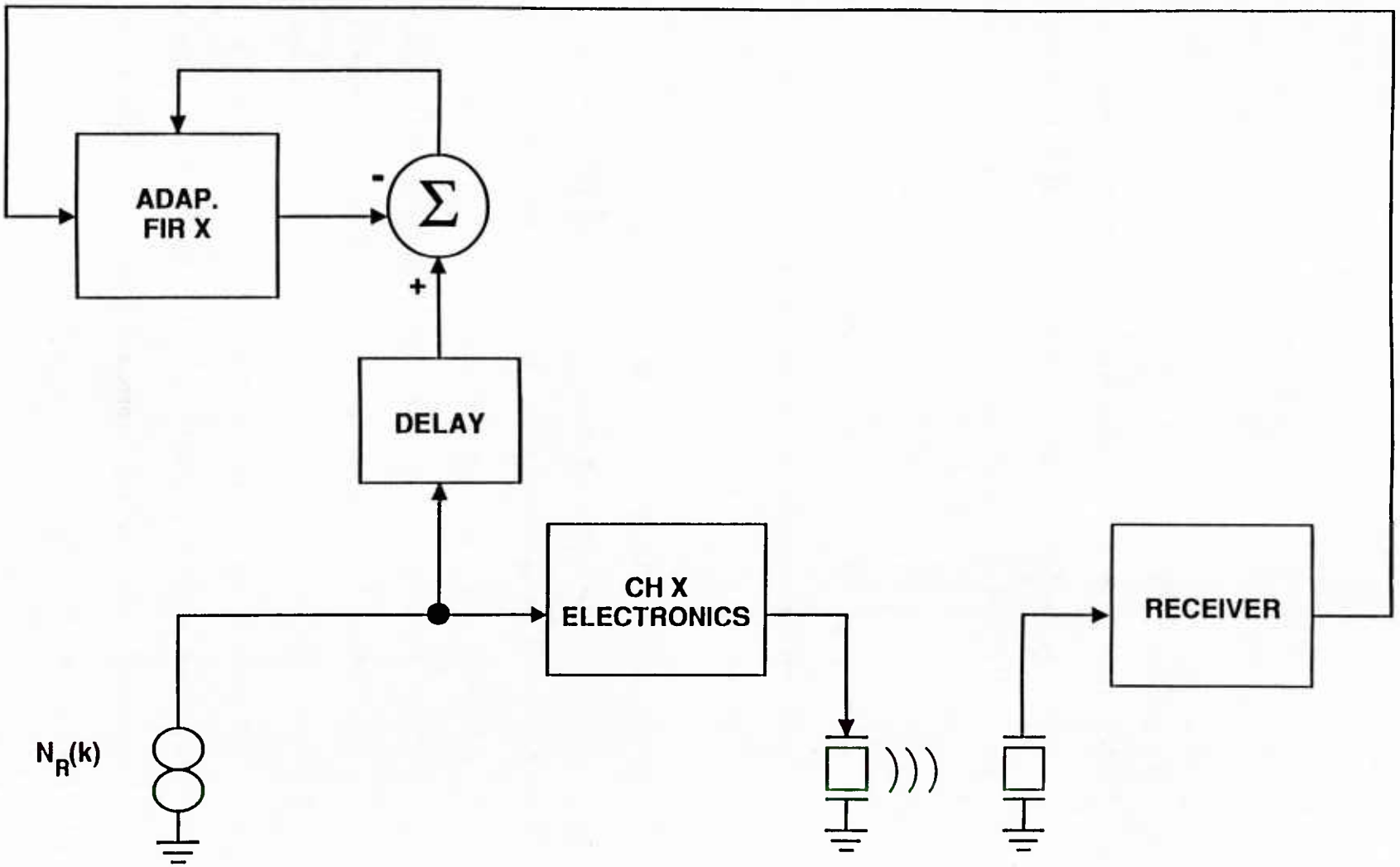

Figure 5. One Channel of Sonar System in ADAPT Mode

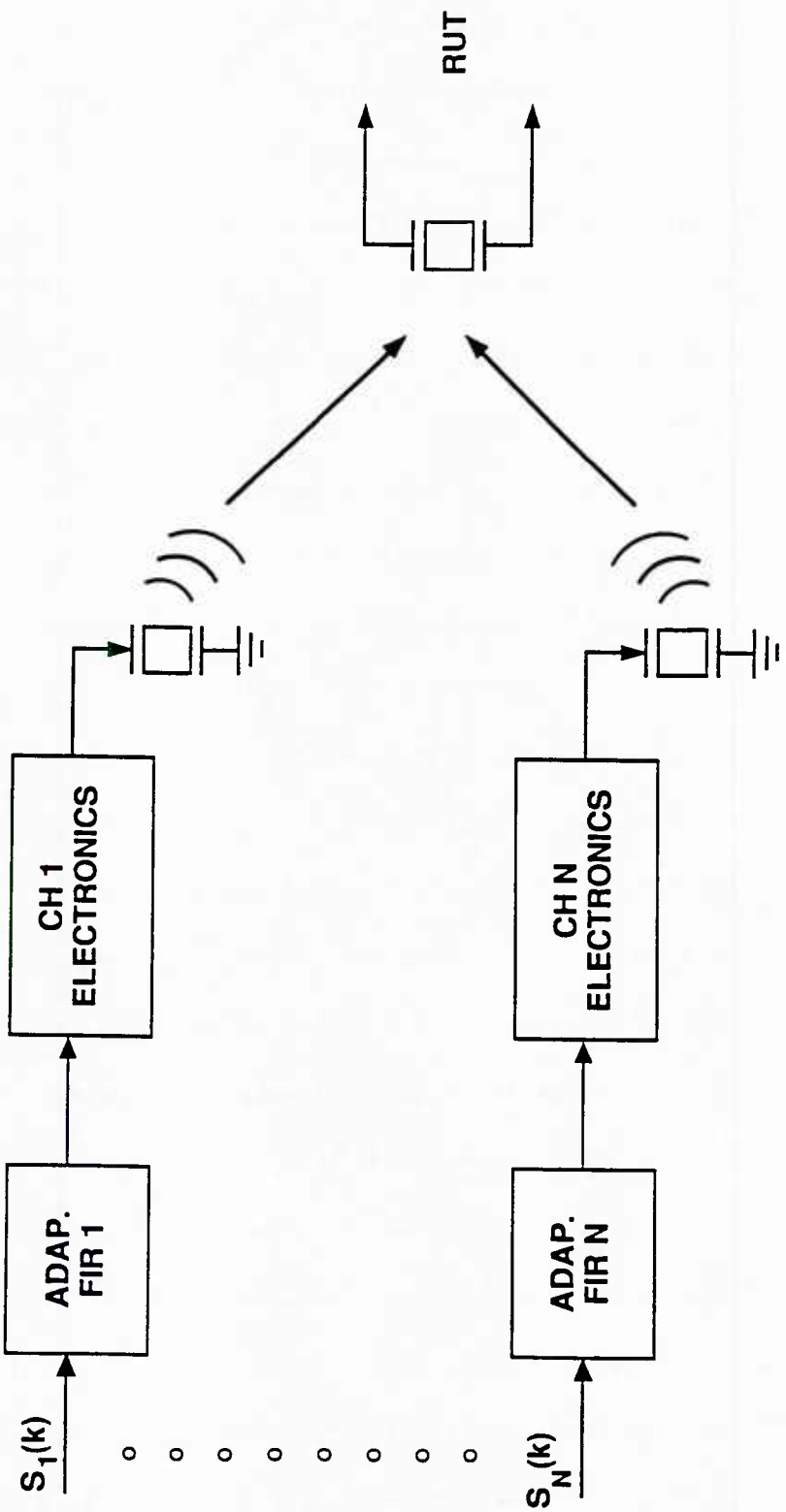

Figure 6. Sonar System in RUN Mode

In Figure 5, one channel of the sonar system is represented in the ADAPT mode. The noise source $N_R(k)$ has a flat spectral density across the system bandwidth and is sampled at f_s. This signal drives the channels' electronics. The electronics consist of a D/A converter, an analog filter to pass a replica of the baseband image at the system's center frequency (f_o), and a power amplifier with matching network to drive the transducer. The matching network is used to shift the transducer's impedance at operating frequency f_o to a more desirable one, thus enabling more signal power in the water. After $N_R(k)$ is transformed to the analog domain where it is filtered and amplified by the electronics, the transducer generates the sonar signal that propagates to the reference hydrophone. The receiver then takes the hydrophone output and provides some filtering and variable-gain-amplification for it. The signal is then digitized at the system sampling rate and passed on to the adaptive filter.

The adaptive filter is a transversal, or FIR type. It is packaged in a single chip -- the Motorola DSP56200 [11]. The tap length of this chip is variable and can be programmed by the user up to a maximum of 256 taps. During initialization procedures, an internal register is written with the desired number of taps. As for the sampling rate, the adaptive digital FIR uses that of the sonar system's, or 9.76 kHz. At this rate, the filter's maximum possible delay time is $256 * (1/f_s) = 256 * 102.5\ \mu S = 26.2$ mS. In general, the delay time is $N * (1/f_s)$, where N is the filter length. In regards to word size, the device accepts 16-bit inputs, 24-bit coefficients, and contains a 40-bit accumulator. The method used to calculate coefficients is the Least Mean Square (LMS) algorithm of steepest descent. The user is required to supply the loop gain only. Since there is no actual convergence speed requirement, the loop gain should be as small as possible such that the weights converge with a minimal amount of self-noise induced in the filter output.

Once the signal has been operated on by the adaptive filter, it is compared to a delayed version of the reference noise source. The delayed version is obtained by passing the reference through a programmable delay buffer. The output of the comparison, or error signal, is then used in the coefficient update algorithm. After sufficient time has been given for the weights to converge, the next channel can be equalized, etc. Finally, after all of the channels are equalized, the system can be put in the RUN mode.

In the RUN mode, illustrated by Figure 6, the adaptive filters are configured as FIRs with their weights obtained from the ADAPT mode. Each is driven by its own $S_x(k)$, the complex, composite signal discussed earlier. The equalized outputs then drive their channel electronics as discussed in Section 1.1. The only difference now is that each channel between $S_x(k)$ and the RUT has the same uniform gain and time delay across the system bandwidth. At the RUT, a weighted coherent sum exists such that the composite signal appears to come from some point within the dimensions of the sonar array. The geometry of the array (a top, side, and frontal view) is shown in Figures 7 and 8.

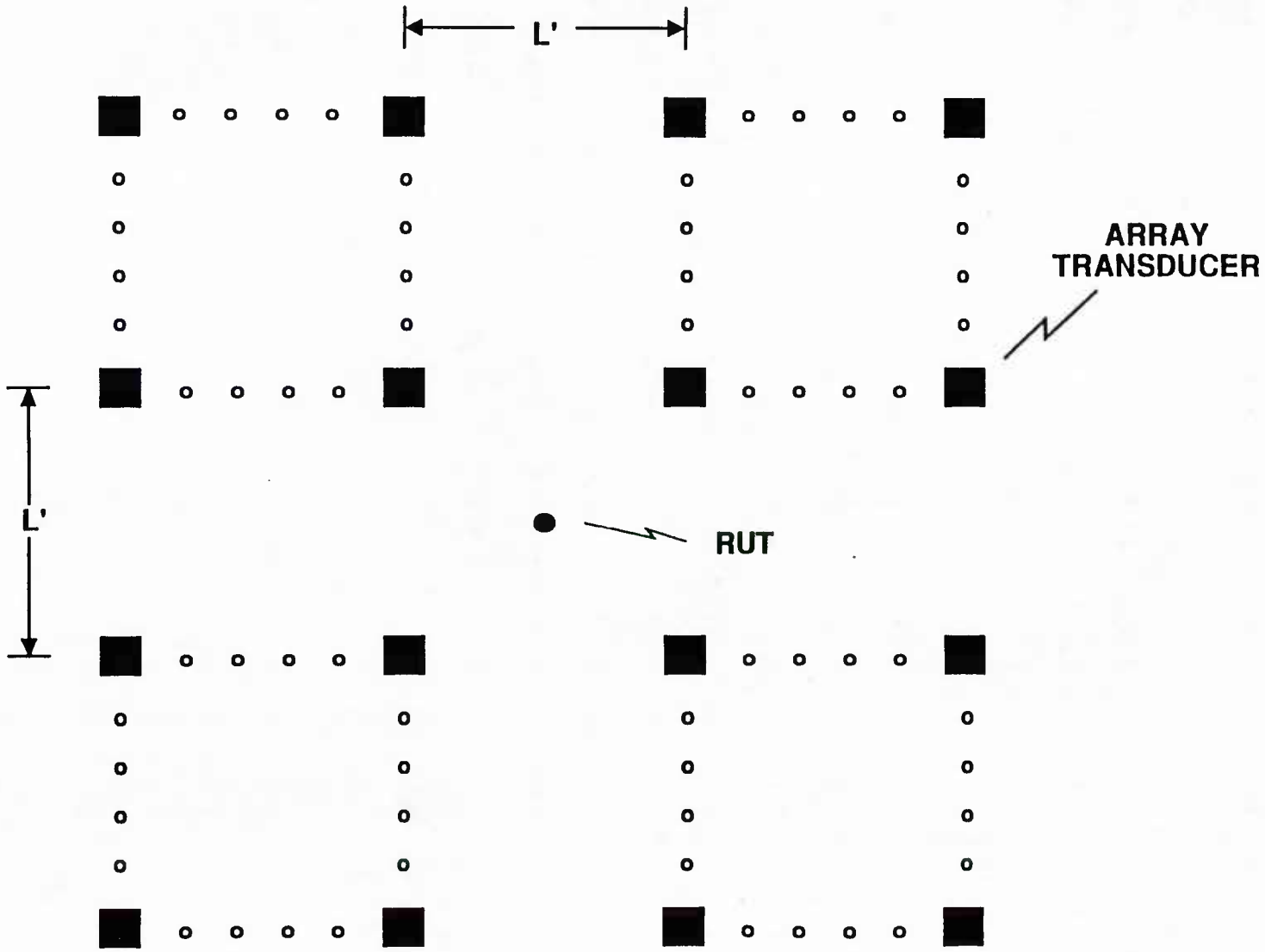

Figure 7. Array Frontal View

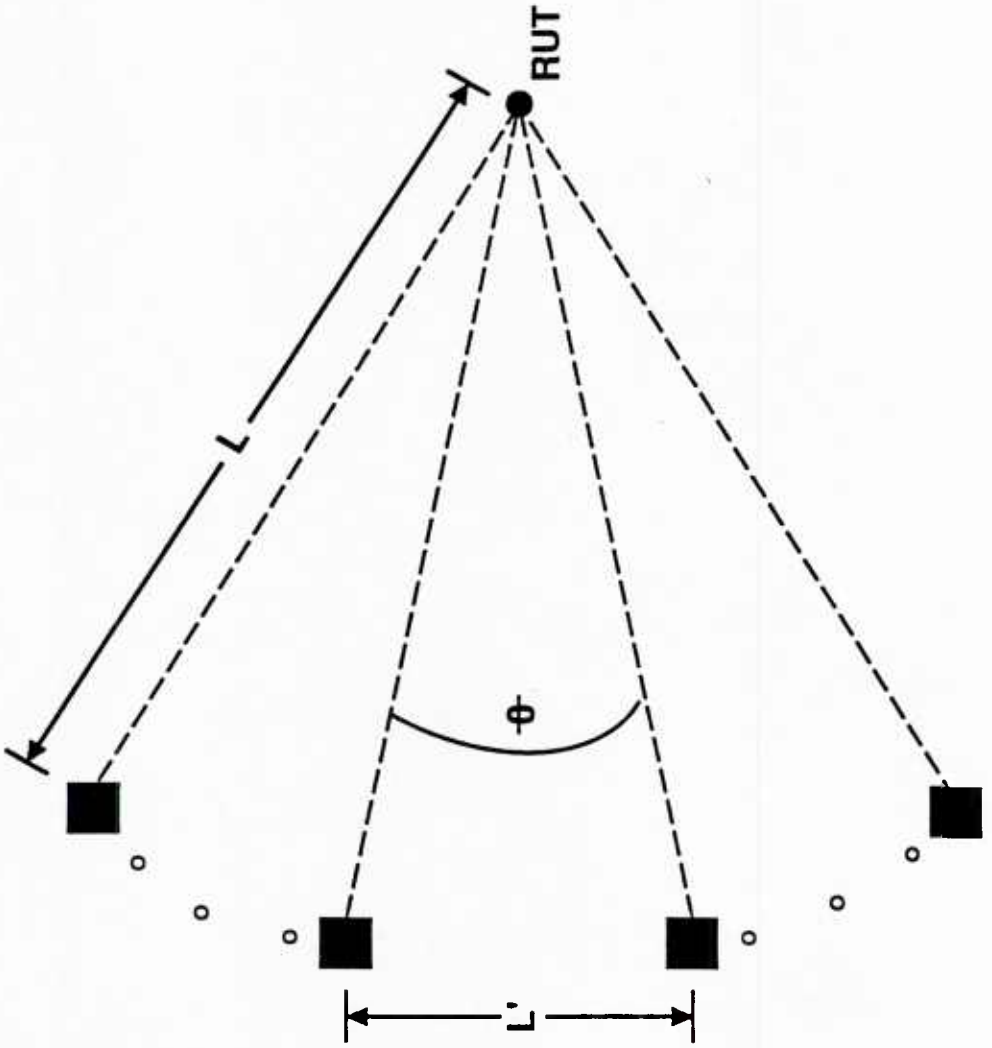

Figure 8. Array Side View or Top View

Chapter 3

EXPERIMENTAL MEASUREMENTS

To verify performance of the proposed solution, it is not necessary to use all elements and channels of the system. The weights for each channel are obtained independently of one another. In addition, since the system is assumed to be linear, superposition applies; therefore, the response seen at the RUT is the phasor sum of the responses at the RUT with each channel operating independently. For simplicity, only the two horizontal elements are used at the top center of the array (see Figure 7). Unless otherwise noted, they henceforth constitute the sonar system. These elements are defined as ELE1 and ELE2 and are driven by CH 1 and CH 2, respectively, as illustrated in Figure 9. The front, top, and side views of this array are shown in Figures 10 and 11, respectively. The appendix contains a physical setup diagram and parts list of components for the following experimental measurements.

3.1 Unequalized Measurements

As indicated earlier, it is of interest to observe the unequalized performance of the sonar system in order to ascertain the amount of distortion present in the system. To accomplish this task, several pieces of data are collected. Two sweeps are done whereby a broadband noise source is moved horizontally across in front of the array by proper amplitude shading of the two system channels and elements in the horizontal plane as a function of time. The first sweep is done with both elements driven in phase, and the second sweep is done with channel 2 driven 180 degrees out of phase with respect to channel 1. Afterwards, frequency domain-magnitude and time delay information is extracted from each channel. In order to generate this data, a broadband

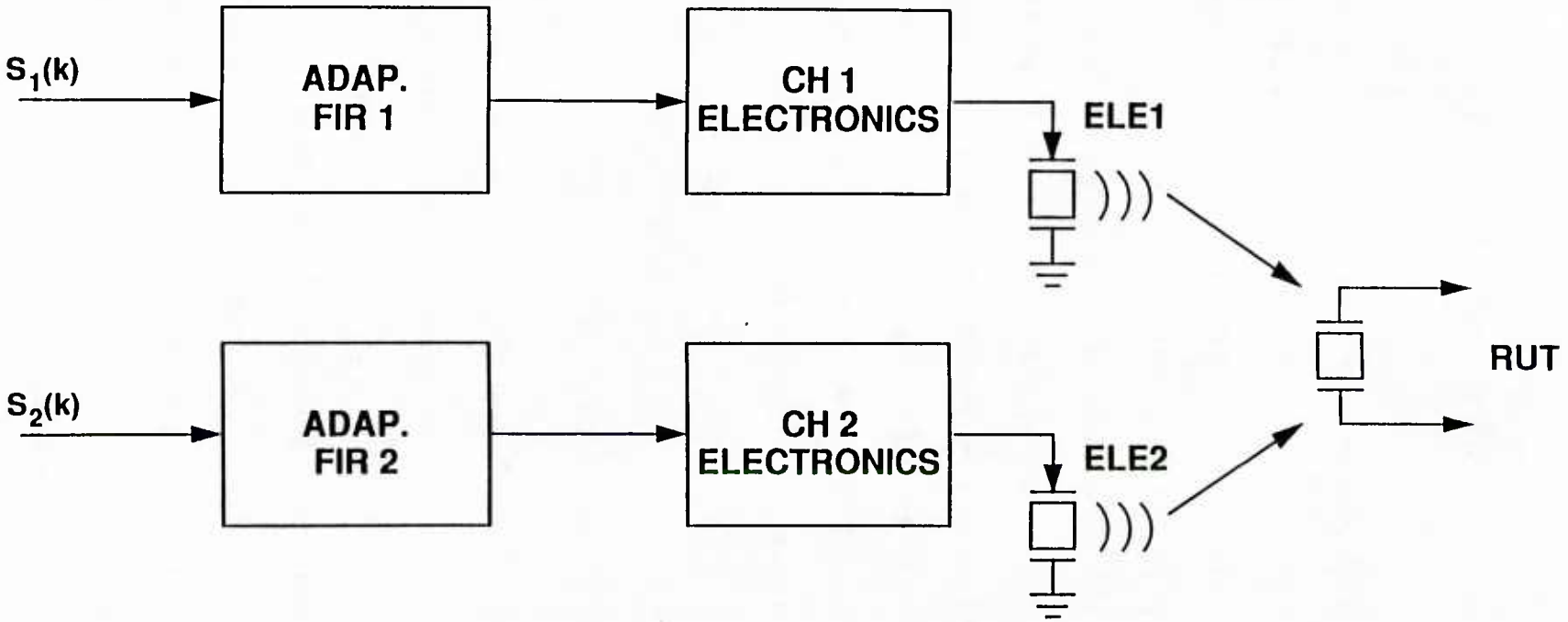

Figure 9. Two-channel Sonar System in RUN Mode

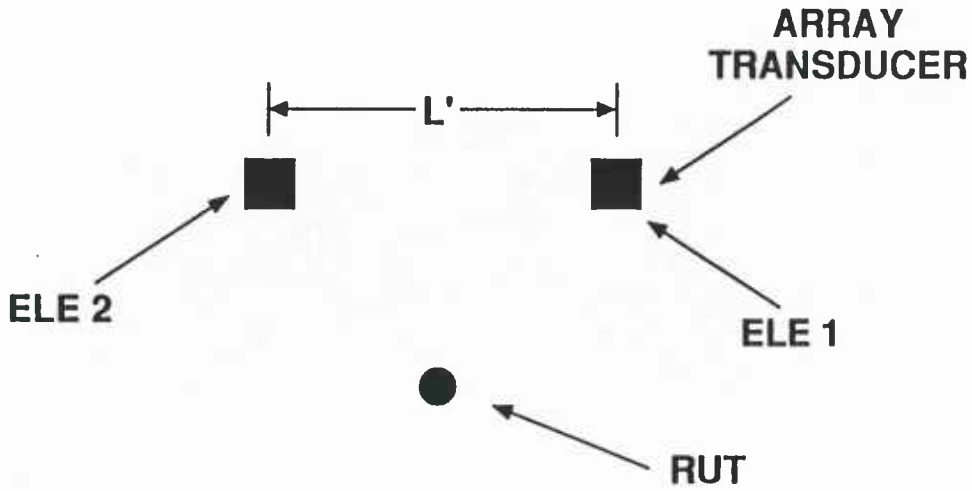

Figure 10. Two-element Array Frontal View

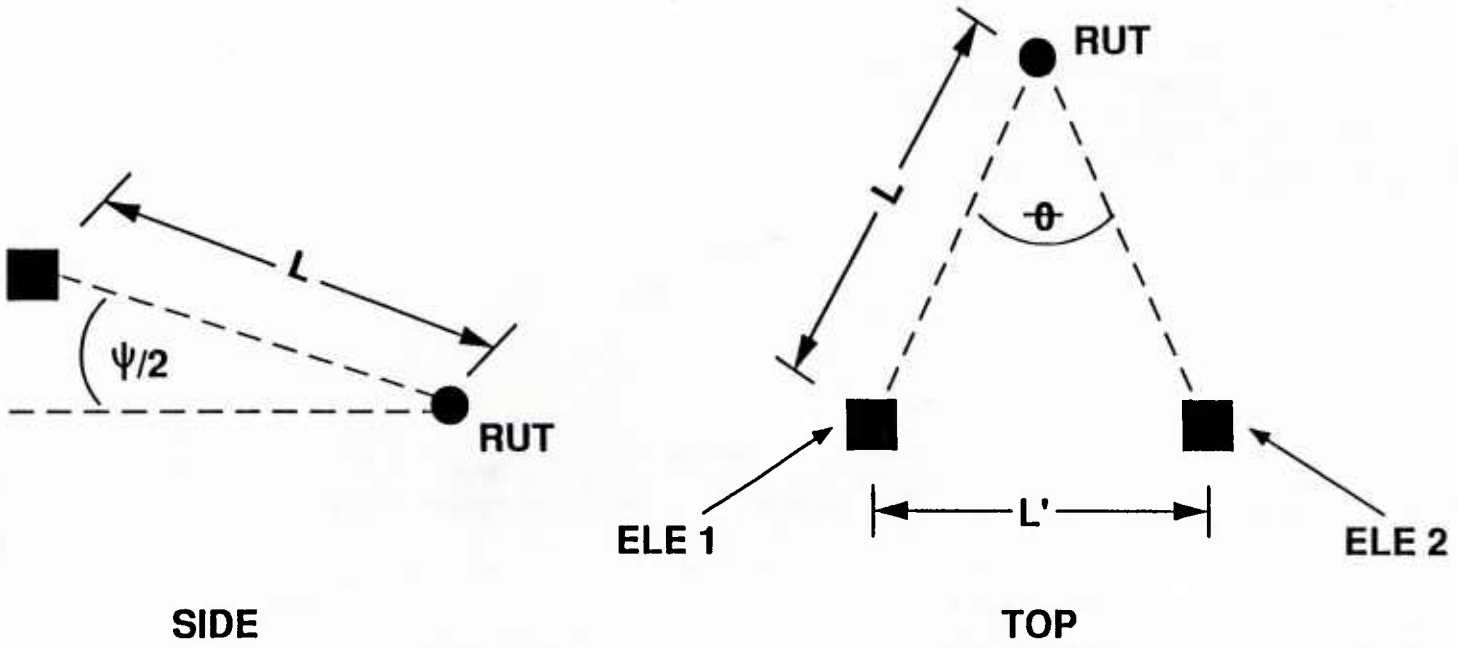

Figure 11. Two-element Array Top and Side Views

noise source again drives each channel. However, this time one channel is driven while the other is off and vice versa. Data recorded at different points in the channel can then be used directly to calculate the desired results.

A detailed description of the measurements and relevant concepts follows. Figure 12, a block diagram of the configuration used in the data collection process, depicts the channels' electronic components. Each channel has the same blocks and will therefore have nominal transfer functions that are identical. Thus, the description provided here applies to both channels. The channel will be denoted by 'X' where X = 1 or 2 and the subscript D, P, or R refers to digital-domain, power amplifier, or receiver, respectively. As before, each channel contains an amplitude-shaded signal source, $S_x(k)$. It contains only broadband noise. A delayed version is output to a D/A converter and appears as a test point, TPØX. The non-delayed signal is output to the power amplifier where it is converted to the analog domain by the D/A converter; all images except the carrier are omitted by the bandpass filter. This signal then propagates through a variable gain amplifier to the matching network and attenuator. The attenuator scales the signal before sending it to the test point, TP1X. The matching network's output drives the element ELEX, sending energy to the RUT. Here, the signal is filtered and amplified by a variable-gain-amplifier, its final destination being test point TP2.

To record data for the sweeps, the broadband source was moved across in front of the array from θ = -8 to θ = +8 degrees (see Figure 13 for the broadband source power spectrum). While the source was moving, the signal was recorded at test point TP2. When the channels are matched and driven in phase, one would expect a constant signal level for the duration of the sweep. However, if there is a difference in channel path lengths, a reduction in level should occur since the signals at the RUT add

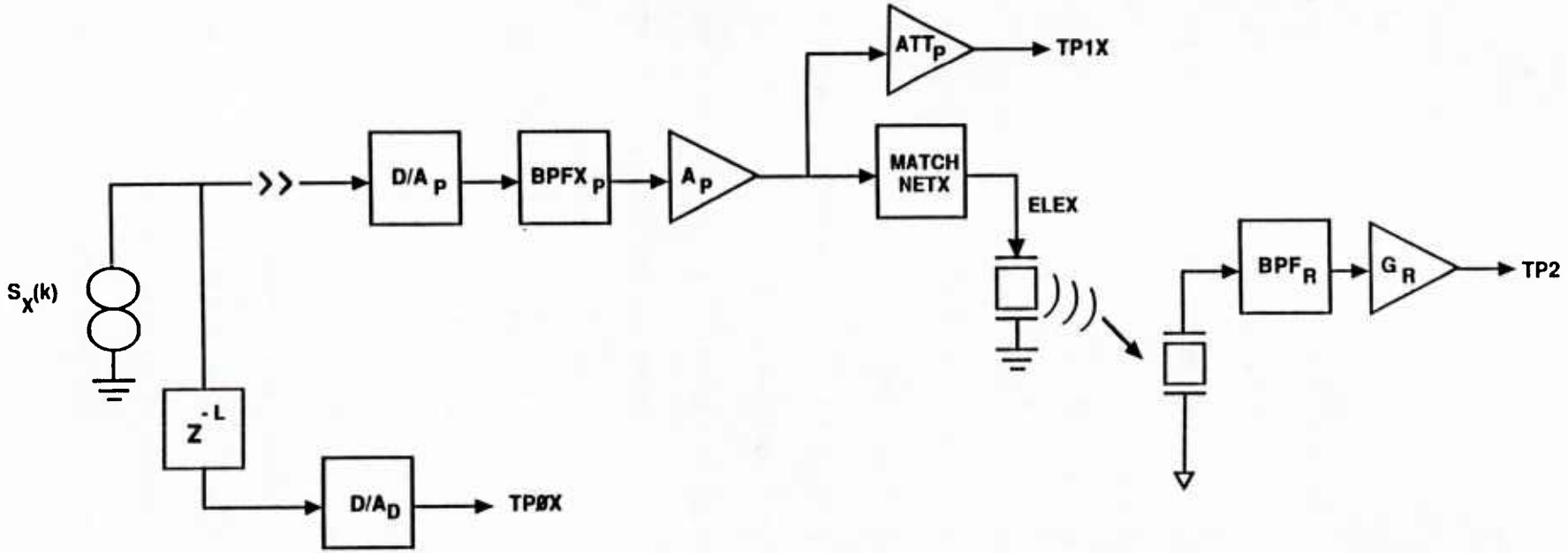

Figure 12. Block Diagram of One Channel of Sonar System Used for Uncompensated Channel Characterization

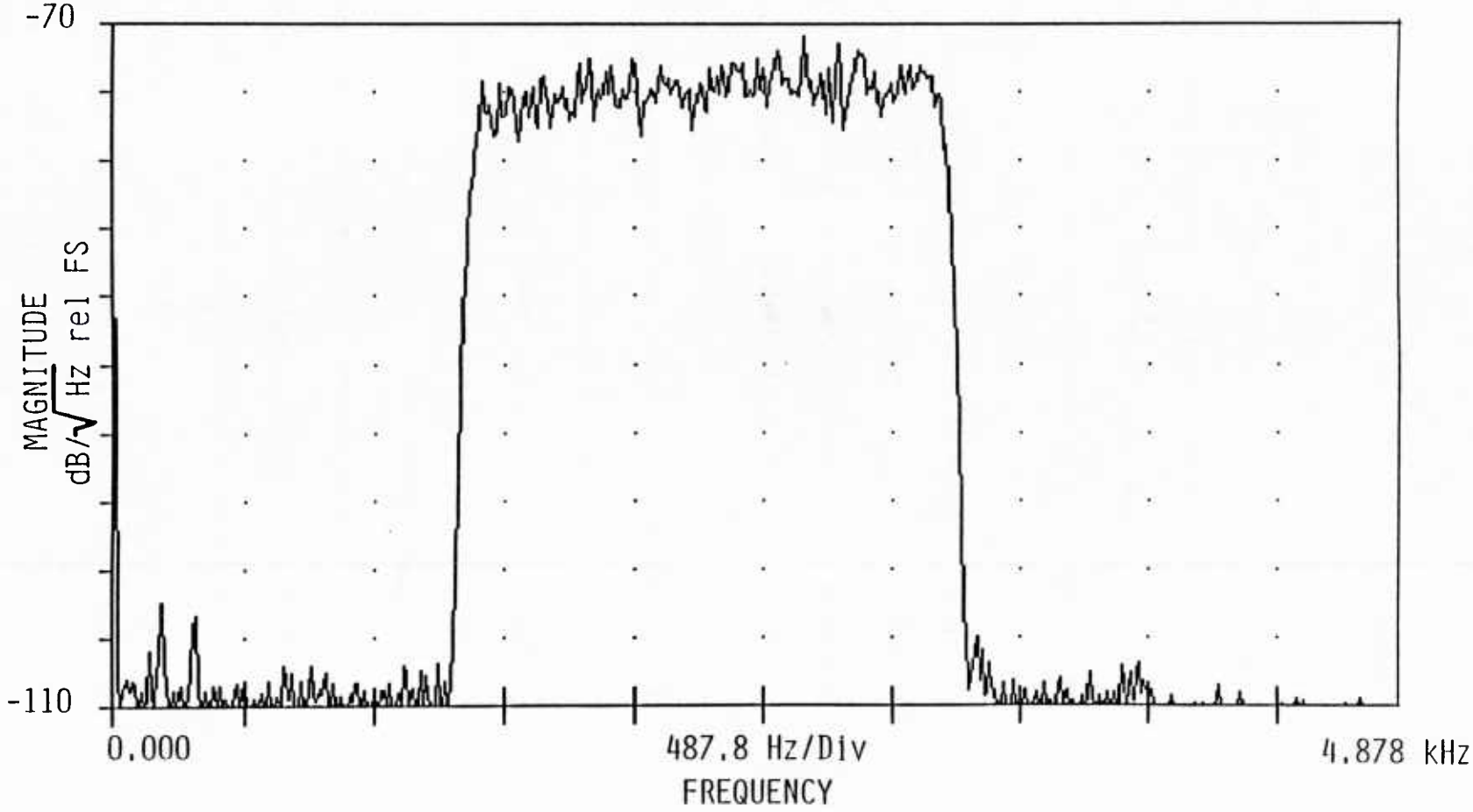

Figure 13. Power Spectral Density of the Broadband Noise Source, $S_x(k)$

orthogonally. On the other hand, when the channels are driven 180 degrees out of phase, the outcome is reversed. Now a reduction in signal level should occur for the matched case and not for the mismatched one.

After the data was recorded, time domain plots were generated for both the in-phase and inverted cases. Figure 14 is a plot of voltage versus time at TP2 for the in-phase case. The ramp up at the beginning of the sweep and ramp down at the end of the sweep is due to the weighting function of the amplitude-shaded array. The shading is done with a triangular window such that the peaks are at the angular locations of the elements relative to the RUT, in this case at θ = -8 and θ = +8 degrees. Notice the null in the center of the sweep. As mentioned above, the delay between the two sources is such that there is destructive interference at the RUT. At this point, the decrease in level is accented the most, by approximately 12 dB. Figure 15 is the corresponding plot for the inverted case. The same basic conclusions can be drawn from this plot. Again, the ramps are noticeable as the source sweeps from less than -8 degrees to greater than +8 degrees. It is interesting to observe how the average level of the envelope is nearly constant between -8 and +8 degrees. This means that the path length differences are such that inverting channel 2 provides a signal highly-correlated with that of channel 1.

In order to get magnitude and group delay on each channel from frequency domain data, recordings were made at test points TP2 and TPØX. Here, the channel being recorded was driven by the broadband source as shown in Figure 13 while the other channel remained inactive. Then, data on the previously inactive channel was recorded in a similar fashion. Afterwards, an FFT was calculated from each channel's data recorded at TP2. The FFT magnitude data gives the frequency response's magnitude information for each channel since the channel is driven with a broadband

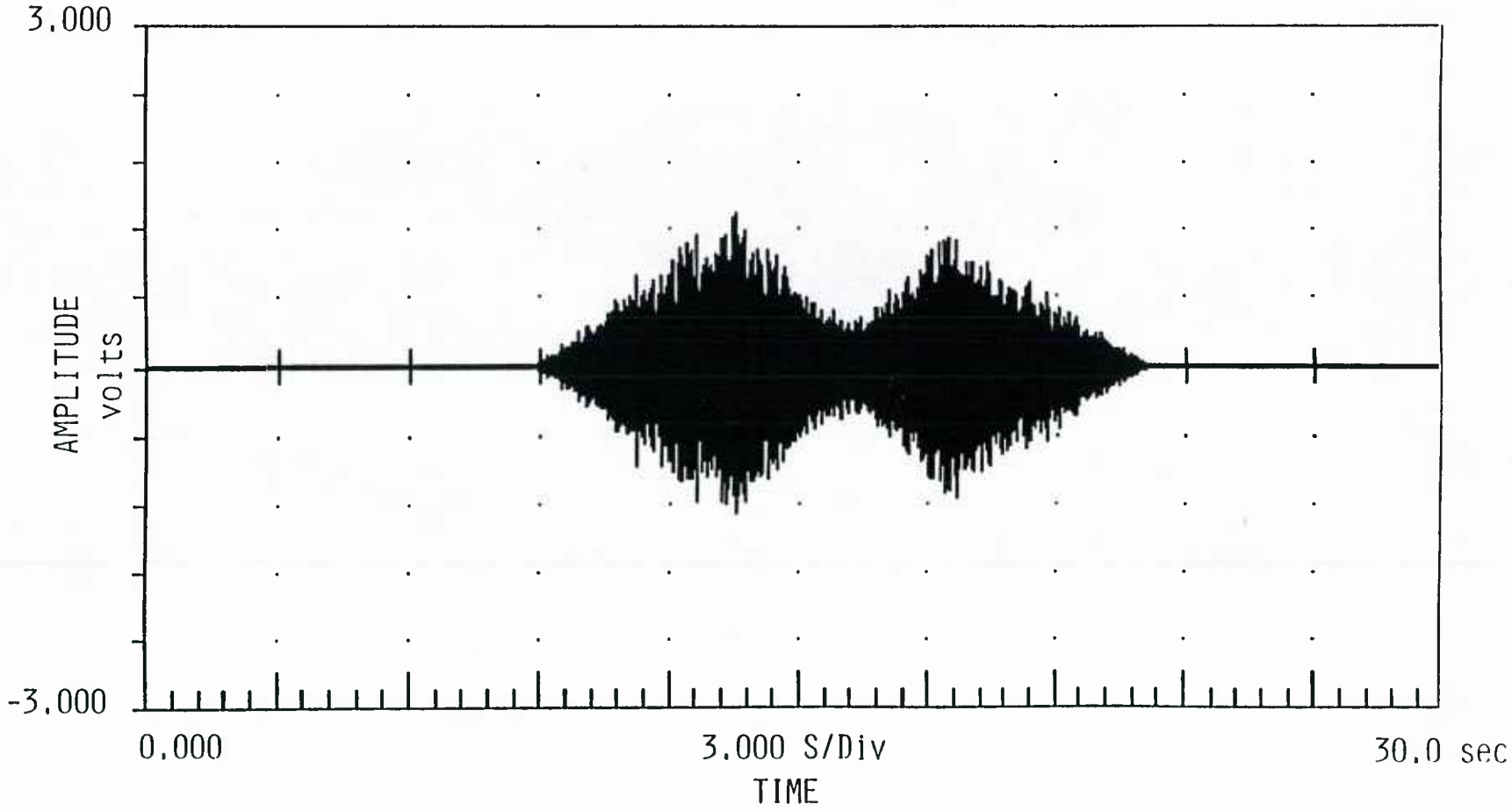

Figure 14. Voltage vs. Time Measured at TP2 for the Uncompensated In-phase Case

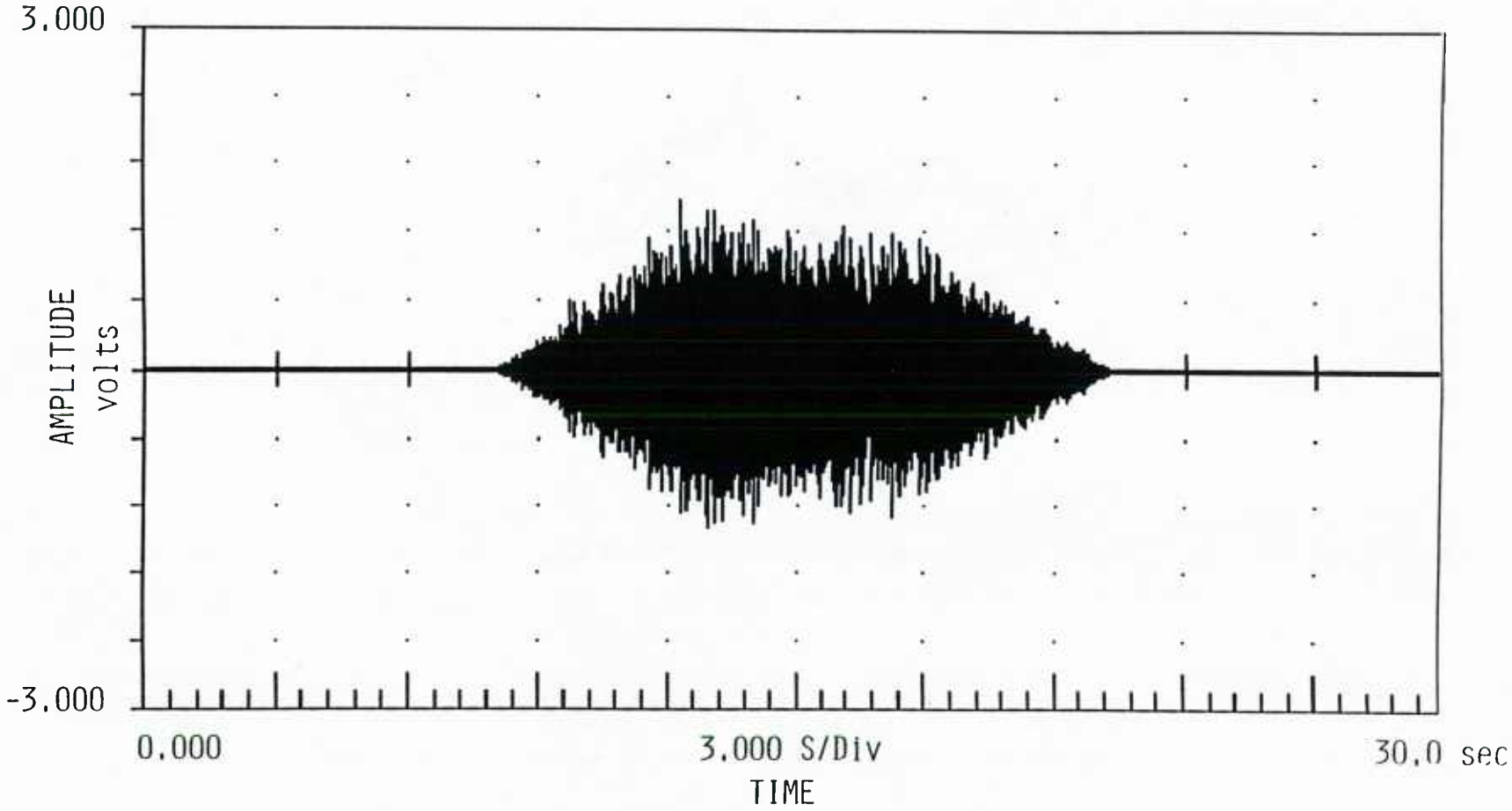

Figure 15. Voltage vs. Time Measured at TP2 for the Uncompensated Inverted Case

noise source that has a uniform spectrum across the system bandwidth. Also, the analog bandpass filter located in the receiver (see Figure 12) has a bandwidth of approximately 2300 Hz. Its presence does not alter the channels' magnitude responses in the system's bandwidth; however, it does affect the group delay.

The frequency-domain magnitude data for channels 1 and 2 can be seen in Figures 16 and 17, respectively. The center frequency of 12 kHz is aliased down to

$$f_{oa} = f_o - f_s$$

where f_{oa} is the aliased frequency. Thus, this frequency is

$$f_{oa} = 12000 - 9760 = 2240\ Hz.$$

The bandwidth is the same as that of the system's, or 1600 Hz. In the passband, the response is upward-sloping, with a total change of about 8 dB. The main elements in the channel are the D/A converter, analog bandpass filter, matching network, driver element, water, and a scaling or gain element (see Figure 12). In the receiver, the responses are uniform across the system bandwidth and can therefore be considered irrelevant. Of the main elements, the analog bandpass filter, matching network, and water have uniform gain characteristics across the frequency band of interest. The D/A converter has a sin(x)/x response given by

$$H(f) = 12\,\frac{\sin(\pi f/f_s)}{\pi f/f_s} \qquad (15)$$

Since the 9760 Hz sampling rate is also the point in frequency where a null appears in this response, it becomes obvious that this mechanism is at least partially responsible for the slope in the magnitude response. In fact, evaluating the above expression at the

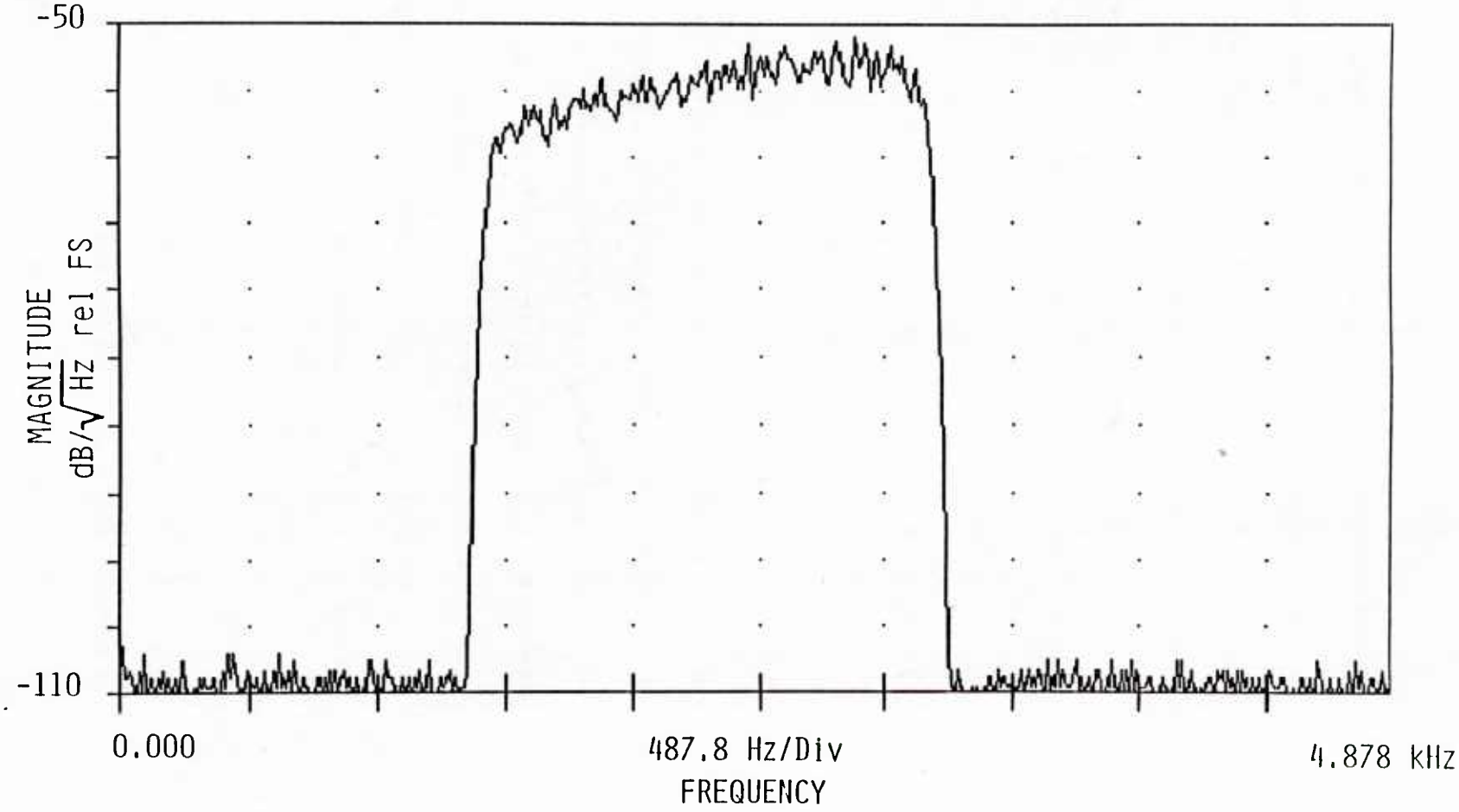

Figure 16. Power Spectral Density at TP2 When Channel 1 is Driven with Broadband Noise Source $S_x(k)$

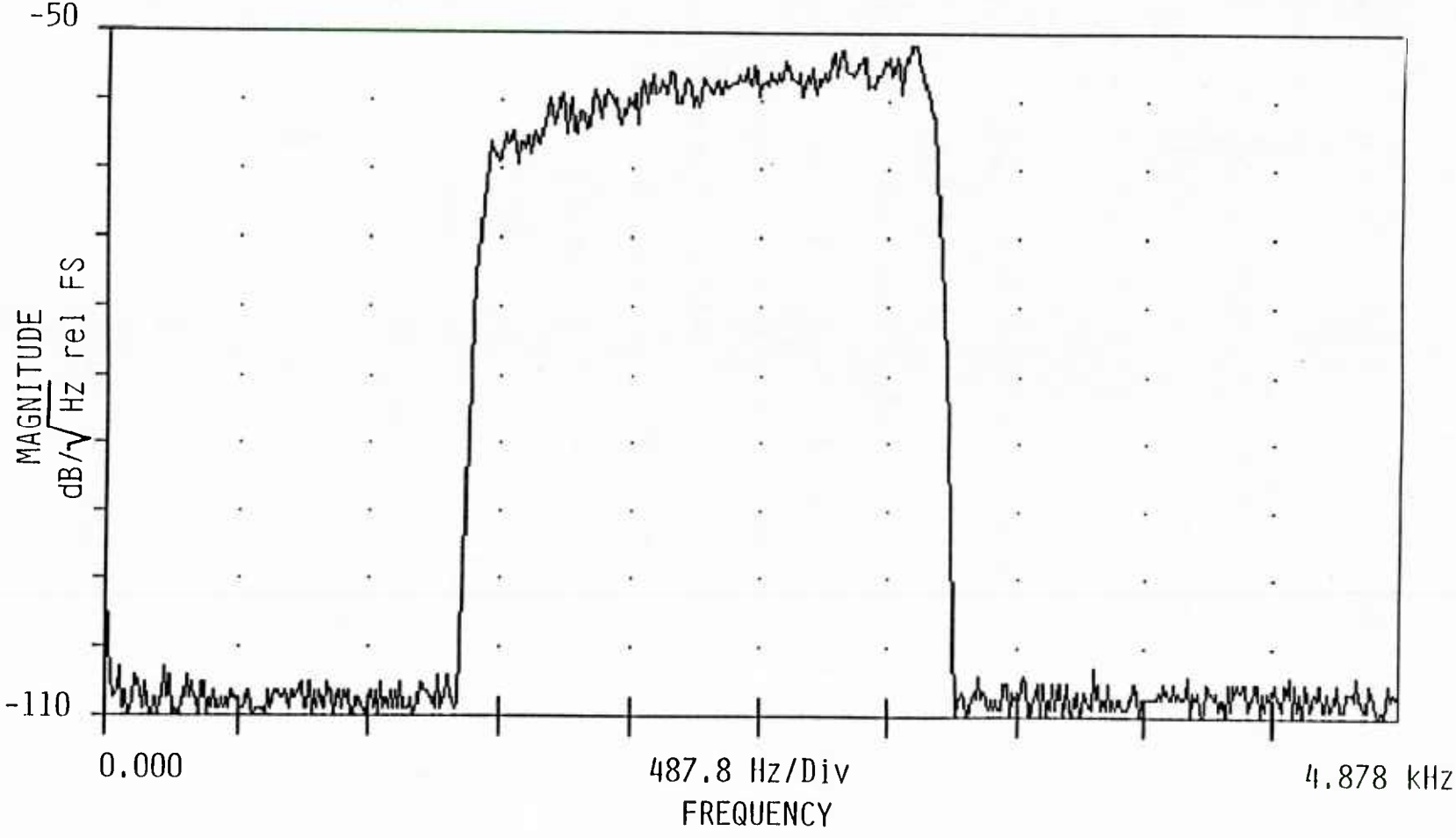

Figure 17. Power Spectral Density at TP2 When Channel 2 is Driven with Broadband Noise Source $S_x(k)$

band edges results in a 4 dB level difference across the system bandwidth. The remaining slope is most likely due to the driver element, whose sensitivity is shown in Figure 18. Due to the similarity of the channels, the magnitude response of channel 2 (depicted in Figure 17) is nearly identical to channel 1's response.

In order to obtain group delay data, the recordings used for magnitude information were used to calculate cross-correlations. The signal at TPØX was correlated with that at TP2 for each channel. A correlation peak should appear at a point in time from which the group delay of the channel can be extracted. Once the delay is obtained for each channel, the delay difference can be calculated. This is the parameter of real concern, not the delay of each channel.

Plots of these cross-correlations described above are shown in Figures 19 and 20 for channels 1 and 2, respectively. The point in time of the primary correlation peak on these plots is of interest. The correlation peak occurs at t = 95.29 msec in Figure 19. Since the reference is at the center of the graph, or t = 104.92 msec, the delay is

$$t_{d1} = 104.92 - 95.29 = 9.63 \; msec$$

However, there is a fixed delay between $S_x(k)$ and TPØX of 128 samples. At a sampling rate of 9760 Hz, this gives a delay of

$$t_f = 128 \cdot 1/9760 = 13.11 \; msec.$$

Therefore, the channel delay is

$$t_{dc1} = t_f - t_{d1} = 13.11 - 9.63 = 3.48 \; msec. \qquad (16)$$

Similarly, the delay from Figure 20 is

$$t_{d2} = 9.9 \; msec$$

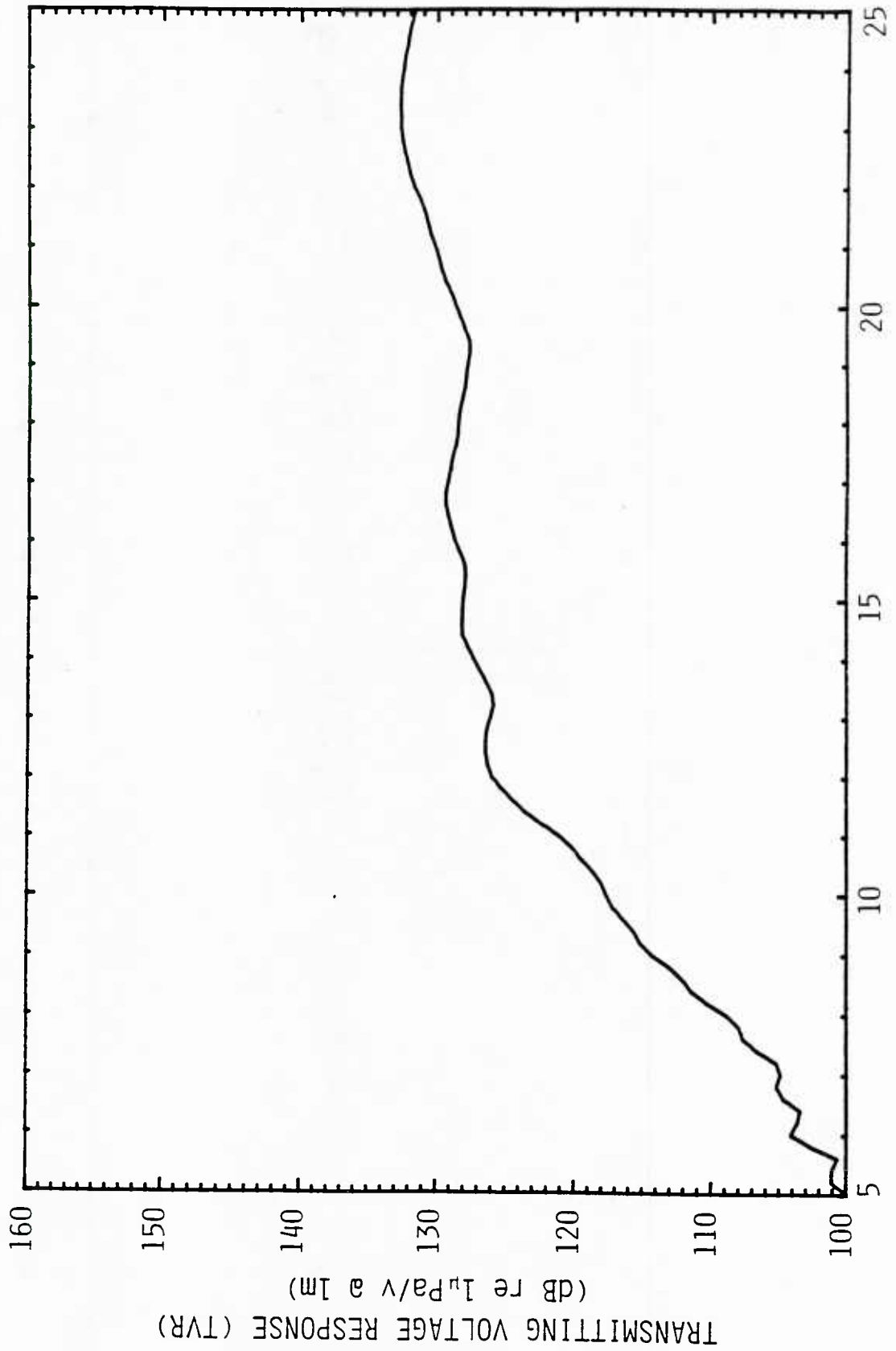

Figure 18. Array Driver Element Transmitting Sensitivity

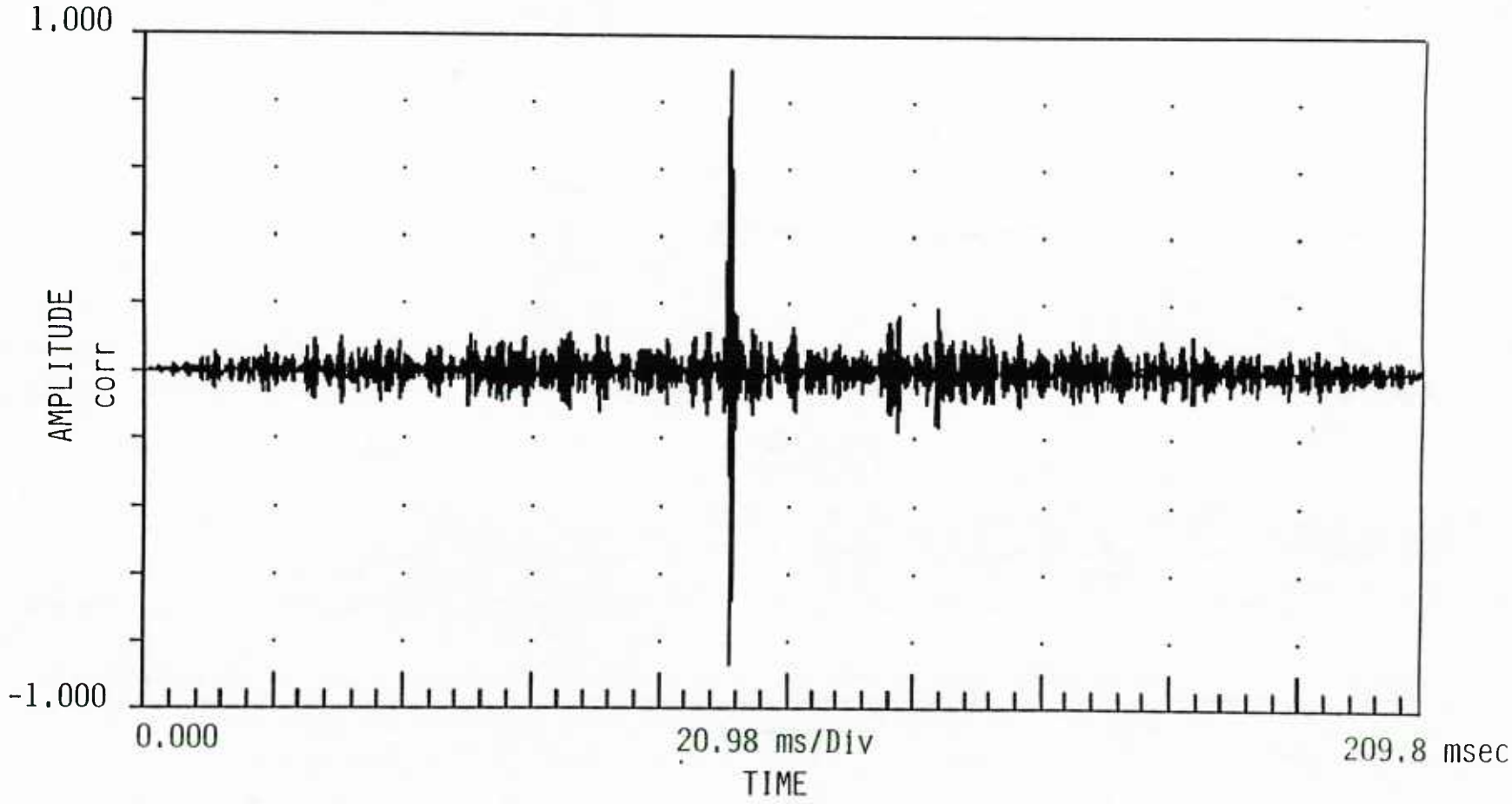

Figure 19. Normalized Cross-correlation Between TPØ and TP2 of Channel 1

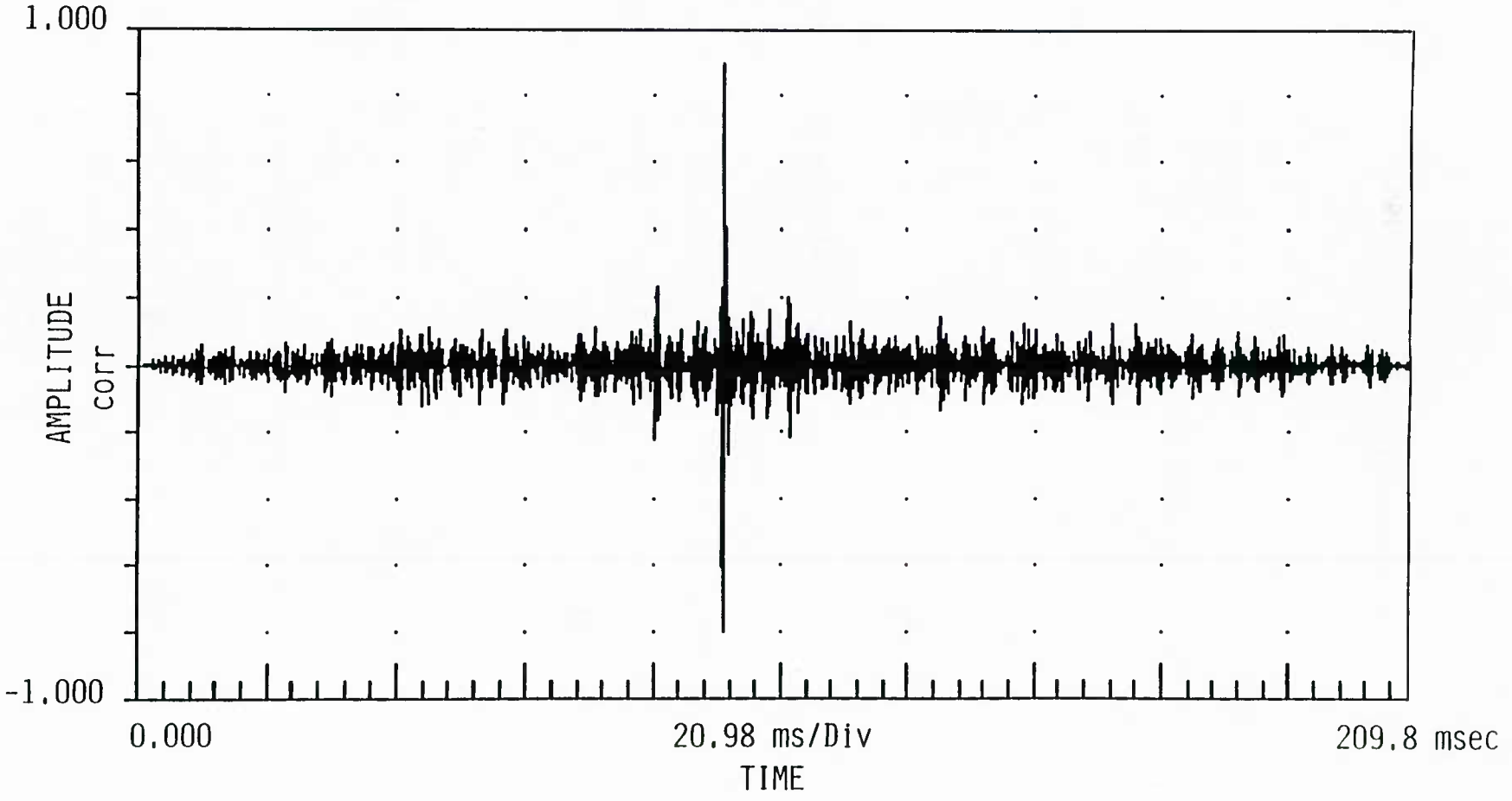

Figure 20. Normalized Cross-correlation Between TPØ and TP2 of Channel 2

which gives a channel delay of

$$t_{dc2} = 3.21\ msec. \tag{17}$$

At this point, the difference in channel delays can be calculated. This is the parameter which must be equalized. It is given by

$$\begin{aligned} t_{dd} &= t_{dc1} - t_{dc2} \\ &= 3.98 - 3.21 \cong 270\ \mu sec. \end{aligned} \tag{18}$$

3.2 Adaptive Filter

In Section 3.1, uncompensated measurements were taken and data presented to provide an overall view of the sonar system and hardware configuration, as well as to establish a feel for the extent of the problem at hand. The crux of the problem can be summarized by observing the passive sweeps, the frequency-domain magnitude responses for each channel, and the relative group time delay between the channels. In summary, the horrendous performance exhibited by the sonar system (5° angle error) necessitates, without question, channel equalization if the RUT is going to measure angles with any degree of accuracy. This section will provide a detailed description of the filter used to solve the equalization problem.

A transversal FIR filter architecture will be used -- a standard practice among equalization applications due to its simplicity. The adaptive algorithm used in the weight update calculations is based on the criterion of minimizing the mean-square error between a reference or primary signal and an estimate of this signal from a secondary source. The estimation is performed via the filter, or more specifically by a finite Weiner Filter [8]. However, since the secondary input statistics which are necessary in the

Weiner solution are not known a priori, an adaptive implementation that recursively approximates the optimum solution is used instead -- an LMS adaptive algorithm. As described previously, this coefficient update calculation takes the form

$$\vec{C}_{i+1} = \vec{C}_i + \Delta_i \vec{S}_i ; i = 0, 1, 2, \ldots$$

where $\vec{C}_i$ is the coefficient vector, Δ_i is the step constant and $\vec{S}_i$ is the instantaneous gradient component,

$$\vec{S}_i = \frac{\partial \xi(\vec{C})}{\partial \vec{C}} \tag{19}$$

Obviously, this algorithm is based on gradient components, specifically those of steepest descent, whereby each iteration moves the coefficients closer to the optimum performance index. This index is given by the minimum value of

$$\begin{aligned} \xi(\vec{C}) &= E[e_n^2] = E\left[(x_n - \hat{x}_n)^2\right] \\ &= E\left[(x_n - \vec{C}^t \vec{y})\right] \end{aligned} \tag{20}$$

where x_n is the reference input, and $\hat{x}_n$ is its estimate which is given by

$$\hat{x}_n = \vec{C}^t \vec{y} \tag{21}$$

and $\vec{y}$ is the vector of present and past secondary inputs. Other adaptive schemes such as the adaptive lattice and Recursive Least Squares (RLS) are also available [3, 10]. Adaptive lattice uses a gradient-descent algorithm on coefficients in a lattice architecture; RLS uses a different error criterion.

The Motorola DSP56200 Adaptive Finite Impulse Response Filter is the actual hardware used to implement the adaptive filter. It can be run in one of two modes: Adaptive FIR or FIR. The Adaptive FIR mode modifies coefficients based on the LMS algorithm of steepest descent, whereas the coefficients are fixed in the FIR mode of

operation. The chip's host interface is an 8-bit data bus, a 4-bit address bus, and associated control signals. This interface is used to communicate various pieces of information between the host processor and the filter. Such items as input and output, loop gain, and coefficients are transferred across this interface to or from the DSP56200. The chip has three pairs of input registers. Each pair represents a 16-bit word composed of two 8-bit words compatible with the host interface data bus path. The three inputs are: 1) an input to a FIR filter in the FIR mode or an Adaptive FIR filter in the Adaptive FIR mode, 2) a 16-bit reference for adaptive applications, and 3) an input for dual FIR operation. In addition, the loop gain is represented by a 16-bit word requiring two 8-bit locations, while the 24-bit coefficients are transferred to internal RAM by three host interface registers. Each RAM location is accessed by an address contained in the RAM ADDRESS register located on the host interface. An 8-bit TAP LENGTH register is also available which enables the user to select the required number of taps. Lastly, the CONFIGURATION register allows selection of operational mode, rounding options, coefficient update disable and other functions [11]. All of these registers are accessed when writing from the host. In the read mode, a different set of registers are accessed. Some of these registers are the same as those already discussed; other important registers are outputs from FIR operations or error signals from adaptive loop operations.

The filter uses a 10 MHz clock as its main time base. In addition, the user must supply a signal synchronized to this time base with a frequency which matches the desired sampling rate. In this case,

$$f_s = 9.76\ kHz.$$

Since the filter's time base is a 10 MHz clock and it performs a multiply-accumulate (MAC) function in one clock cycle, the filter has a maximum throughput time of approximately 100 nsec per tap. Actually, it is a little slower than this due to input/output overhead. For 256 taps, the maximum sampling frequency is

$$f_s(\max) \cong 37 kHz.$$

Obviously, the chosen sampling rate is not going to pose any problems.

The arithmetic unit, bus control logic, coefficient and data RAM exist within the computation unit. The coefficients are stored in a 256-word long by 24-bit wide block of RAM; the data is also 256 words long but only 16 bits wide. The main, or only, processing element exists in the arithmetic unit -- called the MAC section. During a FIR operation, the multiplier accepts 16-bit data from RAM that represents the filter's present and past inputs, as well as the 24-bit coefficients stored in coefficient RAM. Each multiplication output is input to the 40-bit accumulator, where it is added to the previous partial sum. Similarly, a MAC operation takes place in a coefficient update calculation, but with different operators. In either case, at the end of the operation the accumulator is truncated or rounded, depending on the configuration register. This value is then output to the appropriate location. For a FIR filter, the appropriate location is a host interface register. For an adaptive filter, the accumulator is used to calculate the error term first. This result is then stored in the host interface register. The MAC section is then used again to update each of the coefficients h_i by the equation

$$h_i(n) = h_i(n-1) + 2\mu x(n-i) \qquad (22)$$

where $x(n)$ is the present secondary input to the adaptive filter.

3.3 Equalized Measurements

The two previous sections (3.1 and 3.2) discussed the extent of the equalization problem and a potential method of solving the problem, or at least providing for performance improvement (i.e. the adaptive filter). This section will examine the equalization process and the corresponding performance enhancements.

Three fundamental types of experiments were performed: 1) compensation, 2) compensated-channel magnitude and delay, and 3) broadband sweeps. During the compensation experiment, error information from the adaptation process was obtained, as well as the adapted weights. From the error information, convergence properties could be observed while the weights allowed insight into each channel's time and frequency-domain characteristics. With the adaptive equalizers in place, the compensated-channel measurements provided frequency-domain magnitude and time delay response data to enable a comparison of the overall channel performance to that of the uncompensated case. Finally, the broadband sweeps gathered information regarding overall system performance. Again, with the adaptive equalizers in place, a broadband noise source swept horizontally in front of the RUT gave insight into just how well the system was compensated and enabled a comparison of the performance to that of the uncompensated case.

The compensation data was collected on a per-channel basis with the hardware configured in the ADAPT mode, as depicted in Figure 21. As can be seen, the channel devices are the same as those shown in Figure 12; therefore, the discussion in Section 3.1 is relevant here. The only difference is the addition of the adaptive loop which is described in detail in Section 2.0 and illustrated in Figure 5.

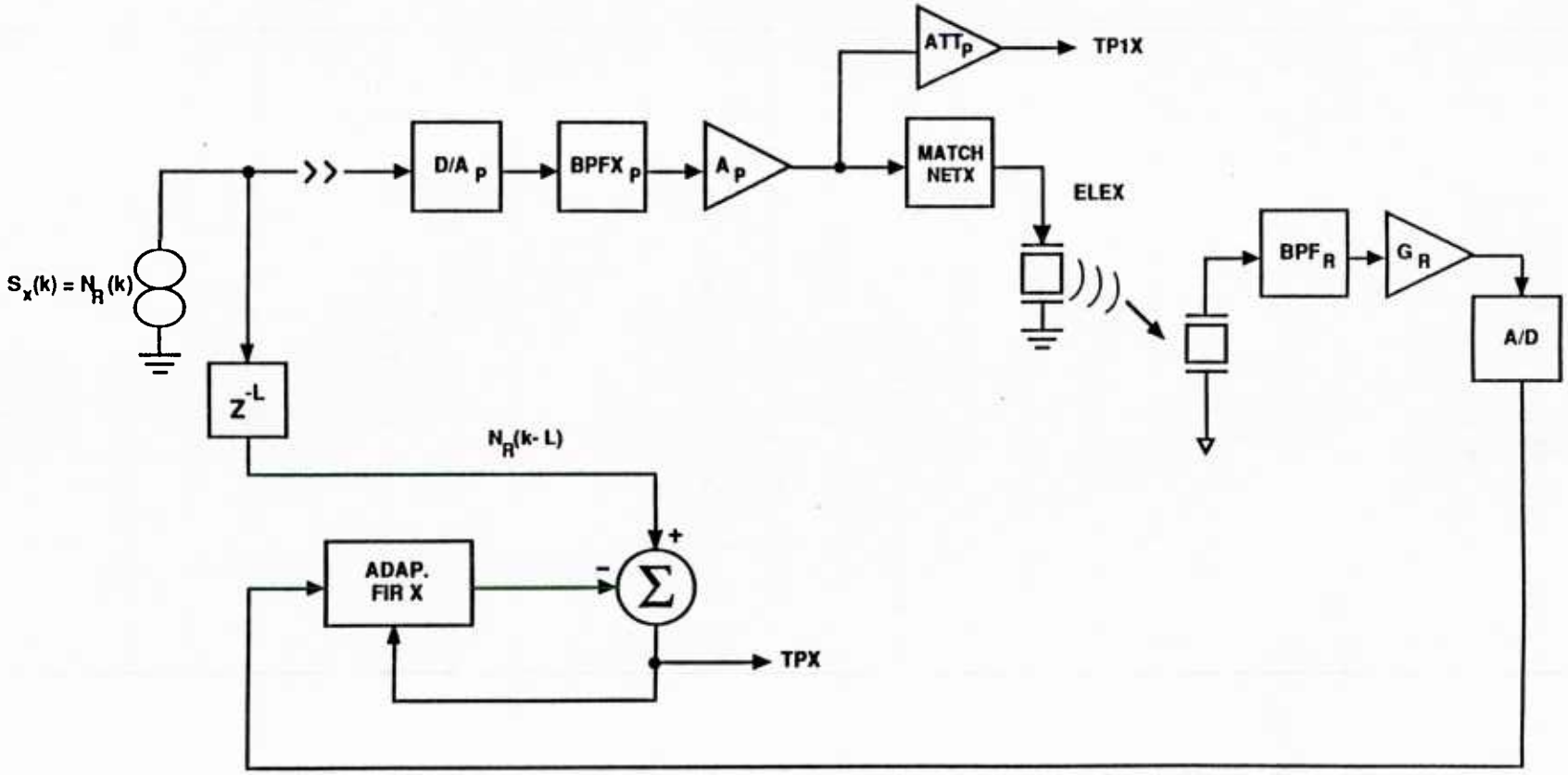

Figure 21. Block Diagram of One Channel of Sonar System Used for Channel Equalization

For the compensation measurements, all of the adaptive weights (256) were first set to 0. Then, the gain A_p was set to 48 dB for both channels. Channel 1 was enabled while its adaptive update capability was disabled. With channel 2 disabled and the reference noise source $N_R(k)$ applied as input to channel 1, the receiver output noise level was adjusted to approximately 20 dB above that of the reference by using G_r. This was done so that a gain of 0.1 would be required by the FIR in order for its output to equal that of the reference level $N_R(k-L)$. After this adjustment, the loop gain μ of the adaptive filters in both channels was set to 0.5.

Once these steps were taken, channel 1's adaptive update capability was enabled and the data at TP1 was recorded. Afterwards, channel 1 was disabled and data was recorded at TP2 during channel 2's compensation. With both channels compensated, the weights were extracted from the filters and committed to storage.

In order to see the effects of varying loop gain on convergence speed, three more sets of recordings were taken as described above. However, in all three cases the gain G_r was increased by 6 dB, while the loop gain was set respectively to 0.5, 0.125, and 0.03125 for the last case.

The data from these experiments is shown in Figures 22 through 25 as normalized amplitude versus time. In all cases, the absolute value of the data record has been taken followed by a 26 msec time average. This data was then scaled to provide a normalized data record. Of interest on each plot is the point in time where the amplitude reaches approximately e^{-1}, or 37% of its initial value at time t=0. Notice that in each figure, this point in time is approximately the same for both channels. If these times are denoted by τ_1 through τ_4 for Figures 22 through 25 respectively, then their numerical values from the graphs are

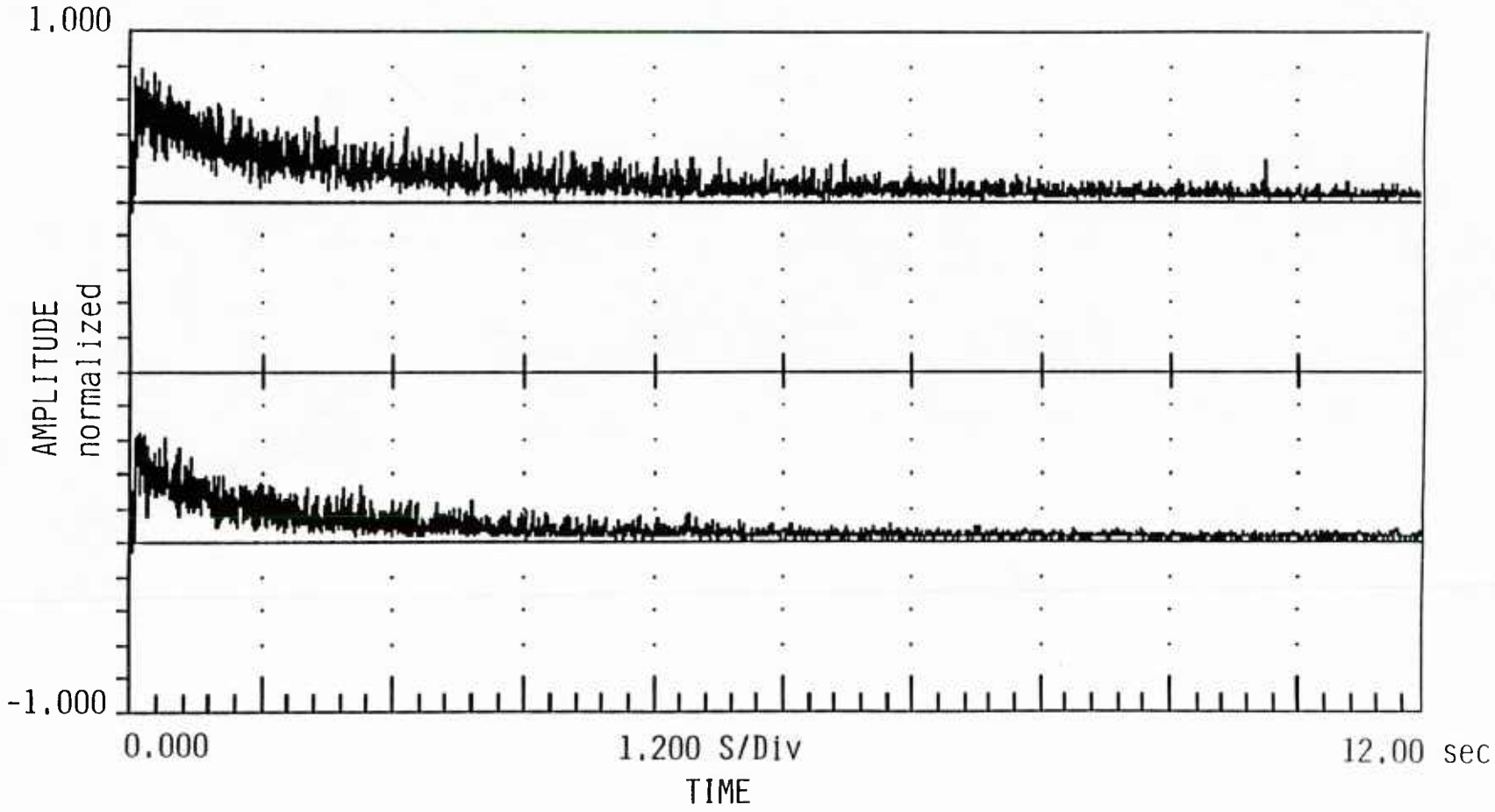

Figure 22. Normalized Envelope of Error Signals During Compensation of Channels 1 and 2

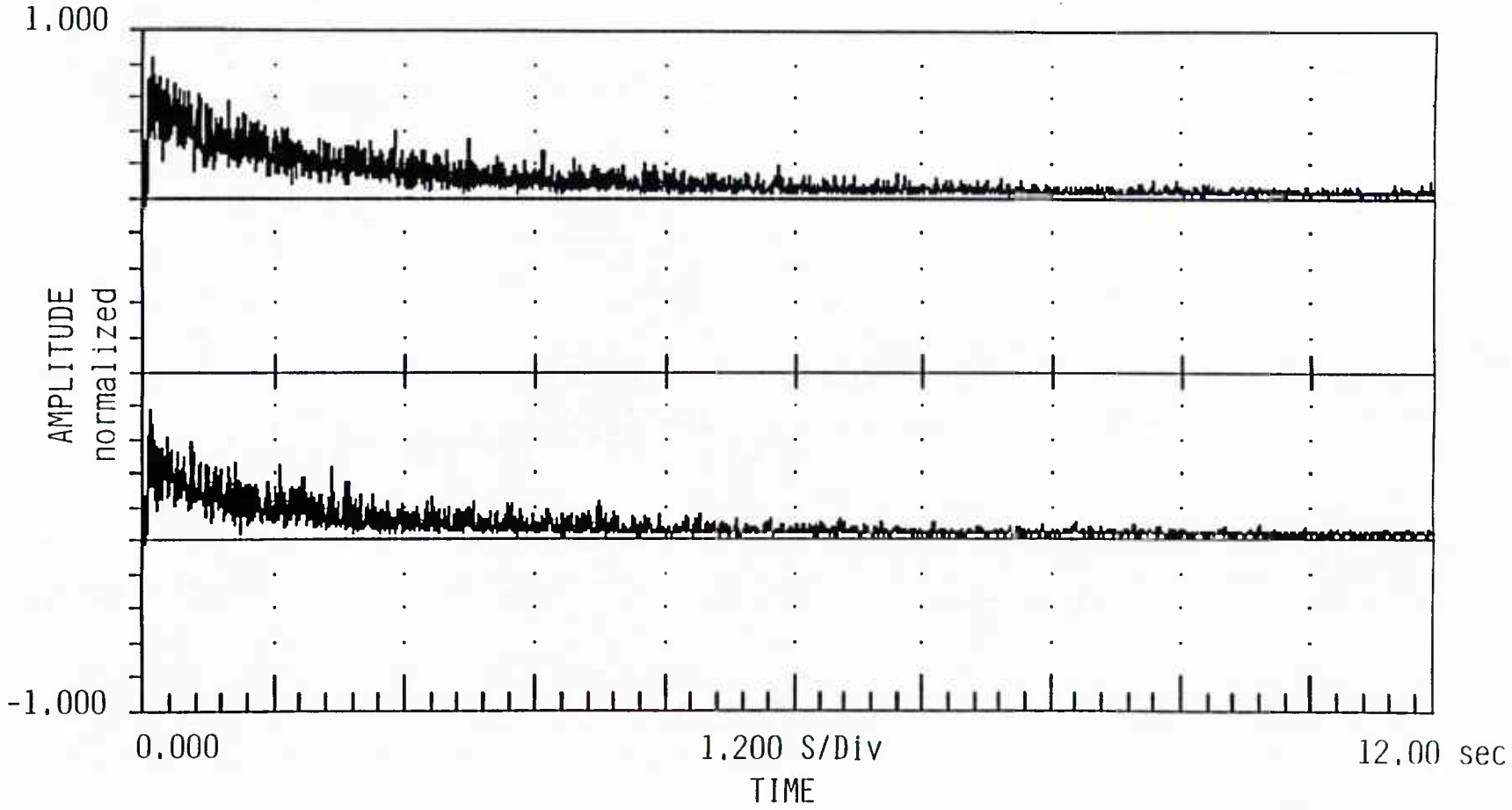

Figure 23. Normalized Envelope of Error Signals with 6 dB of Gain Added and Loop Gain = 0.5

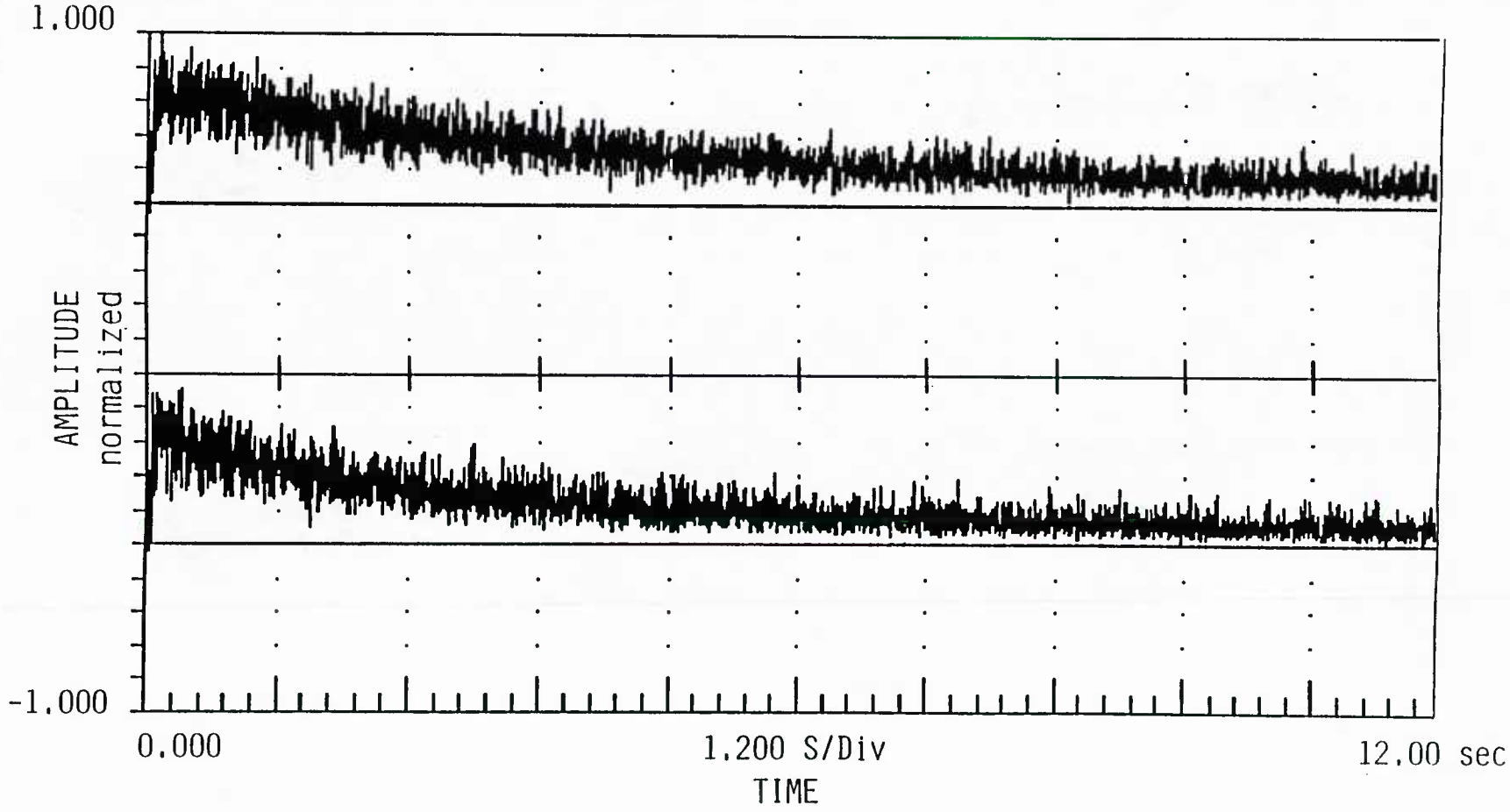

Figure 24. Normalized Envelope of Error Signals with 6 dB of Gain Added and Loop Gain = 0.125

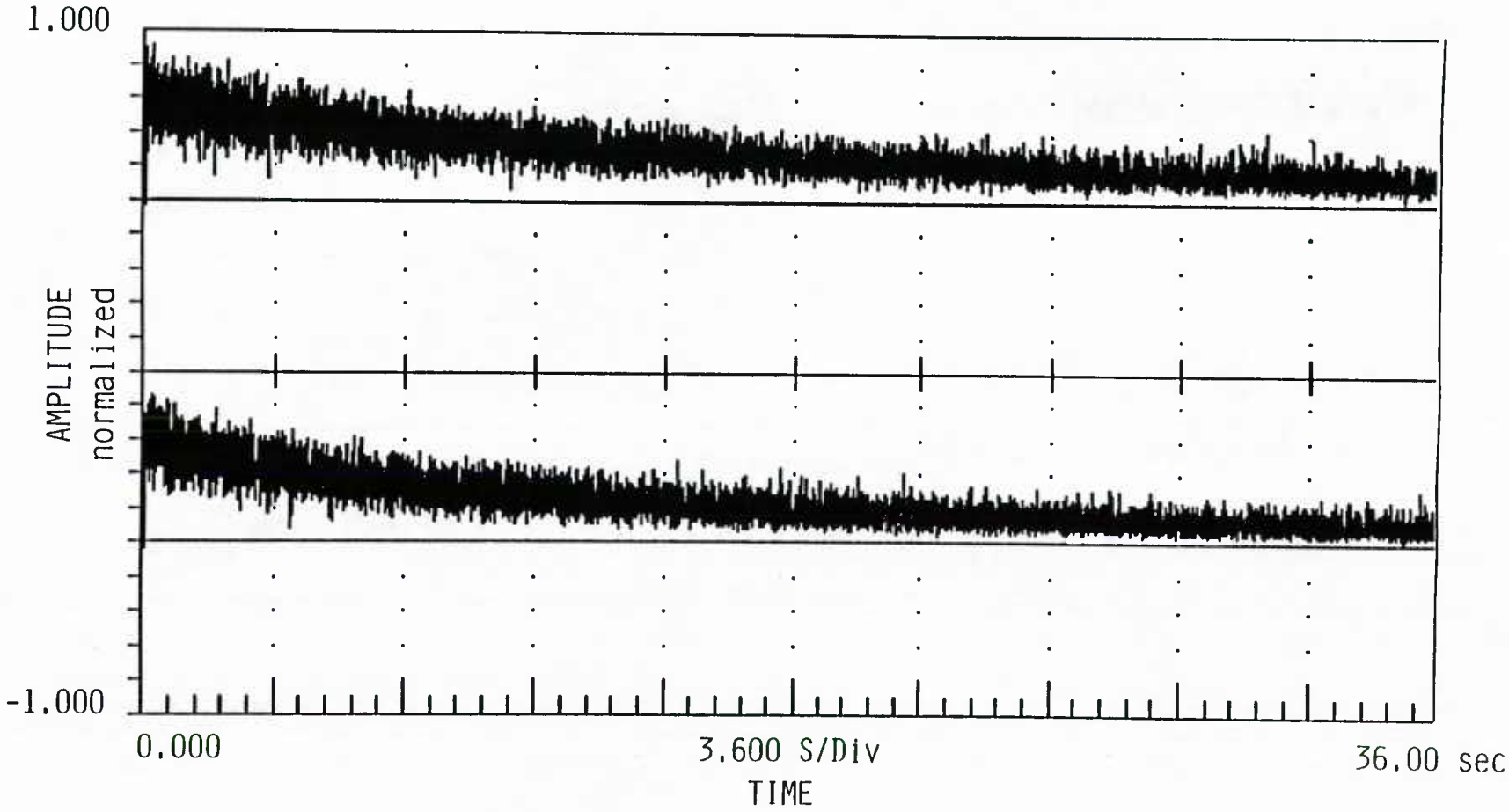

Figure 25. Normalized Envelope of Error Signals with 6 dB of Gain Added and Loop Gain = 0.03125

$$\tau_1 = 1.56 \text{ sec}$$

$$\tau_2 = 1.56 \text{ sec}$$

$$\tau_3 = 6.24 \text{ sec}$$

$$\tau_4 = 23.76 \text{ sec}$$

There is literally no difference between τ_1 and τ_2, even though there is an increase in signal level to the adaptive filter by a factor of two. However, between τ_3 and τ_4 the time gets progressively larger as the loop gain μ gets smaller, as one would expect. Thus, it is obvious that the weights converge to a solution in all of the cases and the time required to do so gets increasingly longer as the loop gain is made smaller.

Characteristics of the compensation filter weights can be seen in Figures 26 through 28. The impulse responses of both channels are shown in Figure 26. These responses are those that correspond to the compensation error signals illustrated in Figure 22. The weights have been normalized to a value of 1, while the horizontal time spans the filter length,

$$256 \cdot 1/f_s = 256 \cdot 1/9760 = 26.2 \; msec.$$

It should also be noted that the time delay of both filters is approximately

$$t_{fltr} = 9.7 \; msec, \tag{23}$$

as seen in the plot where the impulse response peaks are located. This is necessary since the uncompensated channel plus filter delays should equal the fixed delay L/f_s, or from Section 3.1 and using channel 1,

$$t_{dc1} + t_{fltr} = L/f_s . \tag{24}$$

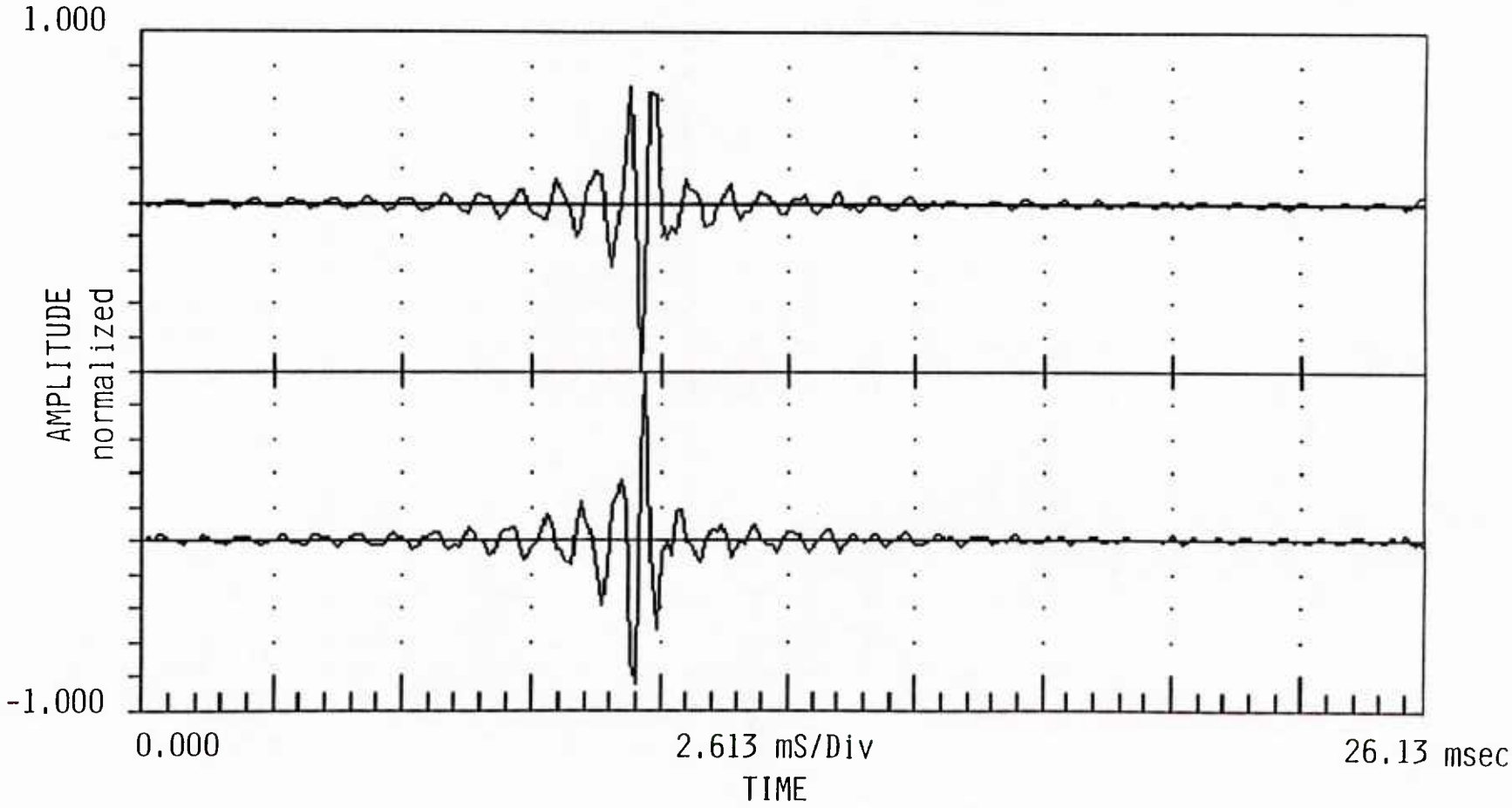

Figure 26. Normalized Impulse Responses of Equalization Filters for Channels 1 and 2

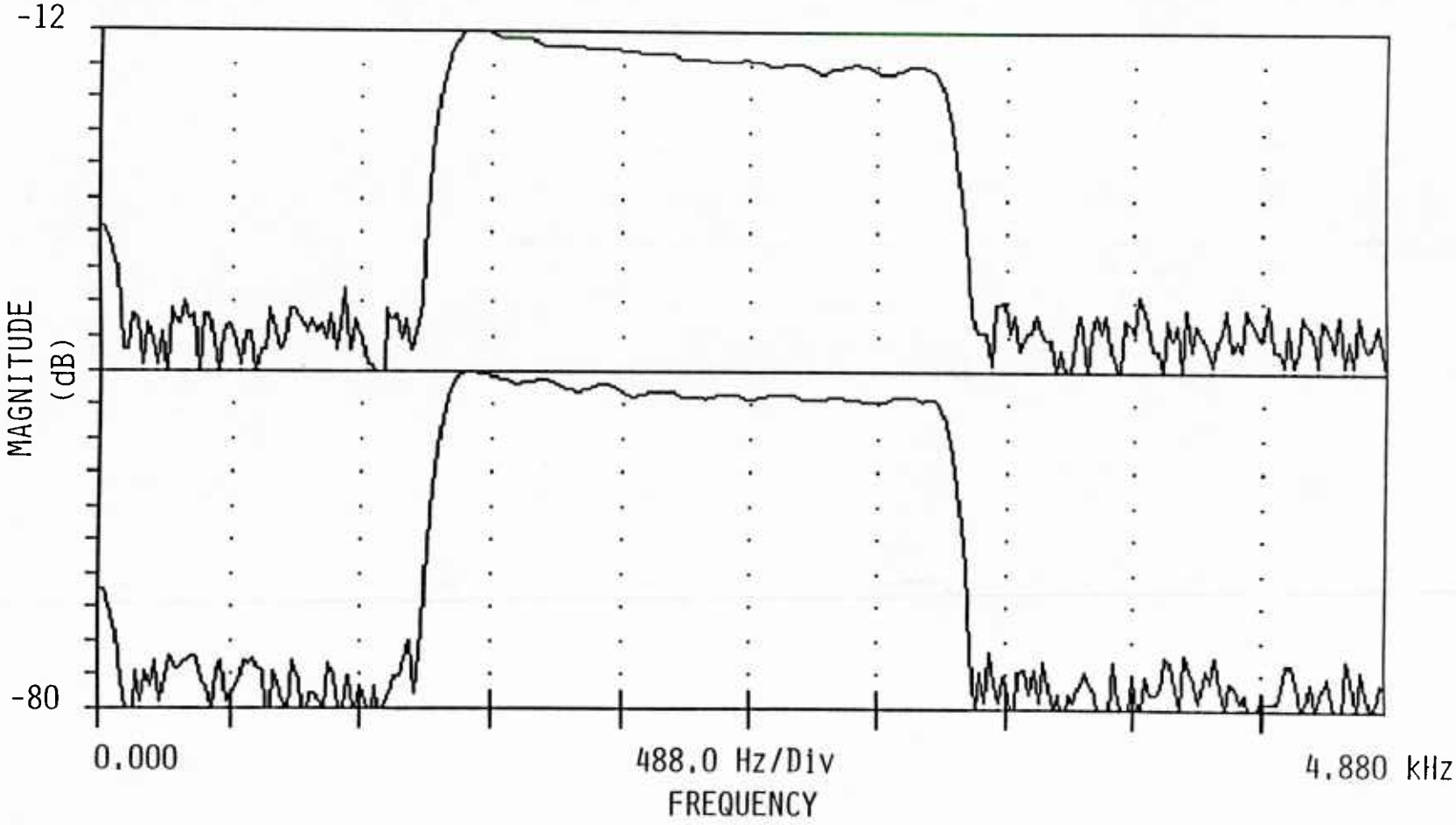

Figure 27. FFT Magnitude Plot of Compensation Filter Weights, Channels 1 and 2

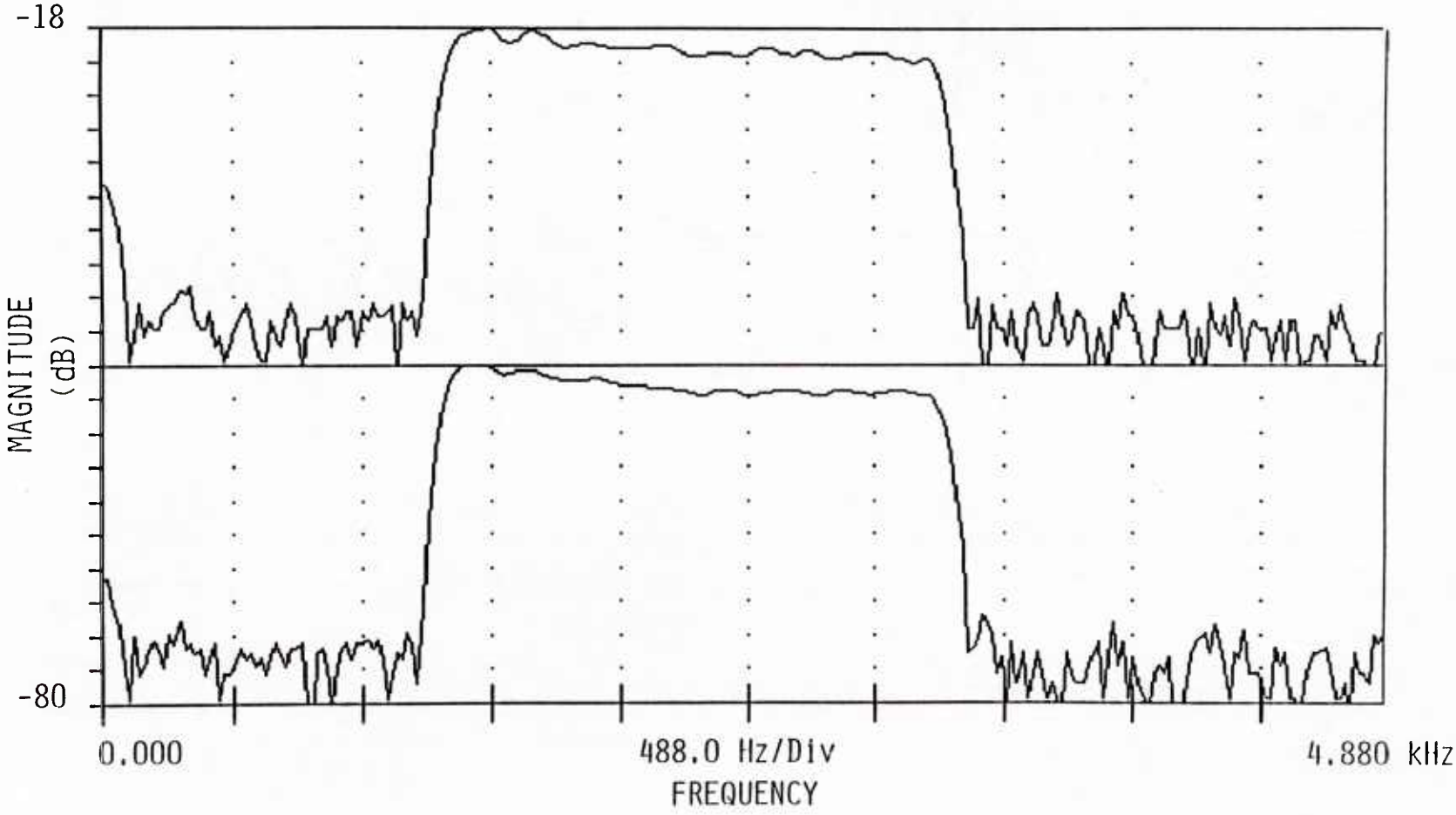

Figure 28. FFT Magnitude Plot of Compensation Filter Weights with 6 dB of Gain Added, Channels 1 and 2

This is indeed the case since

$$3.48 + 9.7 = 13.14\ msec = 128/f_s .$$

Similar results hold true for channel 2 as well. Figure 27 shows the FFT magnitude responses corresponding to the impulse responses presented in Figure 26. Notice that the center frequency appears at 2240 Hz and the bandwidth is close to 1600 Hz. These parameters, as expected, are consistent with the system's parameters.

The passband properties exhibited are probably of even greater interest. Remember in the uncompensated case, the channel magnitude responses had an upward slope with increasing frequency, exhibiting a change of approximately 8 dB across the bandwidth (primarily due to the sin(x)/x of the D/A converters). Here, roughly the opposite occurred -- what one would expect if the composite response was to be flat across the system bandwidth. In addition to the slope, the responses have peaks and troughs in the passband which are attributed to multipath distortion for two reasons. First, the noise source is continuous and contains all wavelengths supported by the system bandwidth. Second, the dimensions of the tank are small enough such that energy at the RUT received via the direct path either constructively or destructively combines with energy obtained through secondary paths within the window of the filter. Finally, Figure 28 contains the FFT magnitude plots of the weights when the receiver gain G_r was increased by 6 dB. As expected, these two plots are very similar, with the exception of the 6 dB decrease in gain from Figure 27 to Figure 28. This gives the system designer some versatility in choosing channel gains. When compensating, the reference gain should be set at the required setting in order to achieve the desired gain from the adaptive weights.

After the compensation data was obtained, the architecture was rearranged as shown in Figure 29 to record the compensated channel magnitude and time delay data on a per-channel basis. This arrangement is identical to that shown in Figure 12, except for the insertion of the Adaptive FIR whose weights were recently obtained from the compensation experiments. With the noise source $S_x(k)$ applied to channel 1's input and channel 2 disabled, data was recorded at test points TPØ1 and TP2. The roles were then reversed; i.e., channel 1 was disabled and the source was input to channel 2. This time, however, the data was recorded at test points TPØ2 and TP2.

Processed data from these measurements exist and are shown in Figures 30 and 31. Figure 30 presents the frequency-domain magnitude response of both composite channels, i.e. fully compensated. As before, the center frequencies and bandwidths are equal to those of the system. However, notice that in the passband the gain is uniform throughout. This is precisely what is desired for a compensated channel -- a uniform gain throughout the system bandwidth that can be adjusted by varying receiver gain during the compensation phase.

Figure 31 illustrates that both channels now have equal time delays. These plots are normalized cross-correlations between data recorded at test points TPØX and TP2. Notice that the correlation peaks occur at the center or reference, in this case a zero-second delay with respect to the reference $N_R(k\text{-}L)$. This is necessarily the case since it has already been established that the channel delay plus filter delay equals the fixed delay. Since the cross-correlations are performed between the delayed reference and the reference delayed by the channel plus the filter, there must be near-zero delay between the two in order for the adaptive process to converge. As can be seen from the figure, this is the case for both channels 1 and 2. More importantly, however, the correlation

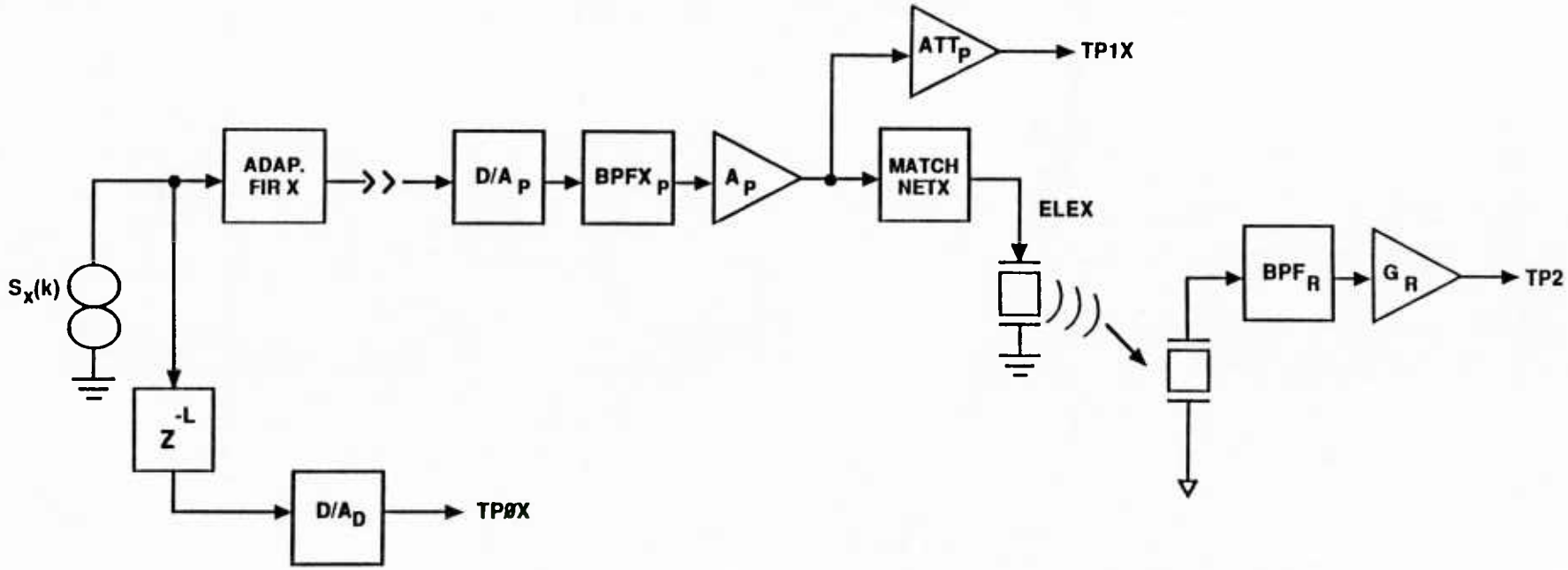

Figure 29. Block Diagram of One Channel of Sonar System Used for Compensated Channel Characterization

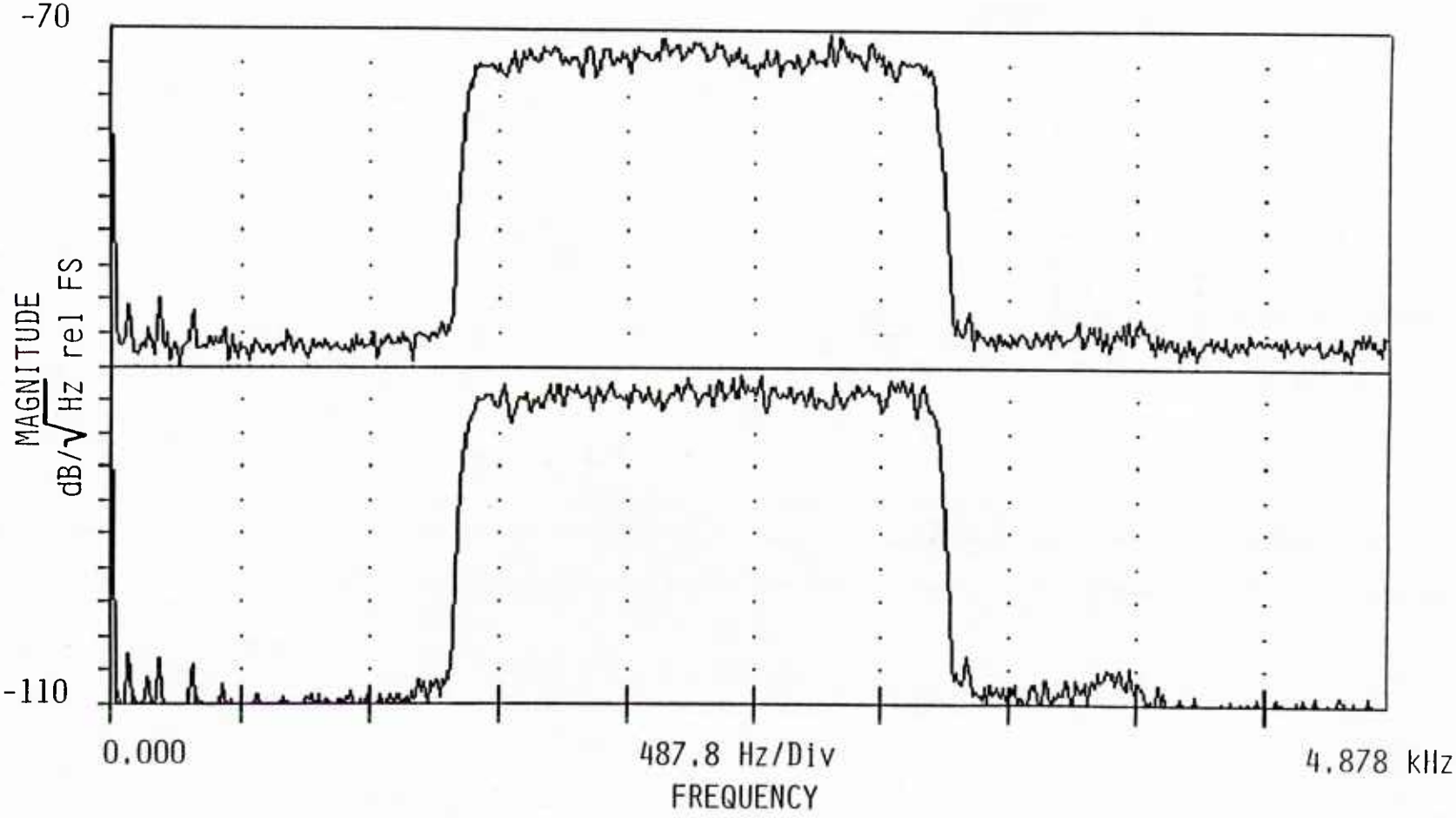

Figure 30. Power Spectral Density at TP2 When Channel is Driven by Broadband Noise Source $S_x(k)$ -- Top: Channel 1, Bottom: Channel 2

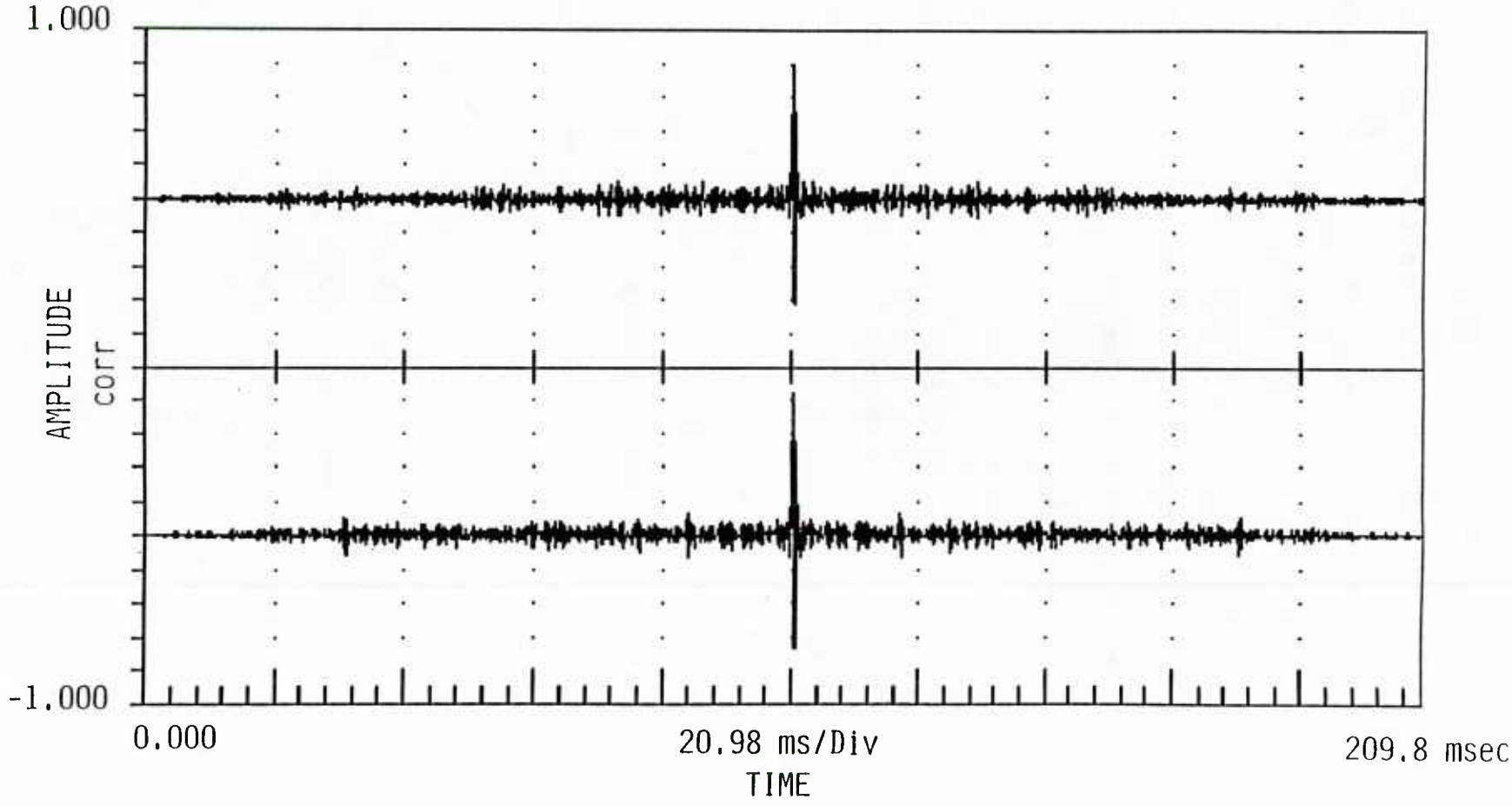

Figure 31. Normalized Cross-correlations Between TPØX and TP2 When Channel is Driven by Broadband Noise Source $S_x(k)$ -- Top: Channel 1, Bottom: Channel 2

peaks for both channels occur at precisely the same time. This means that there is a corresponding zero time delay between channels, which is another desirable feature of a compensated sonar system. Since uniform frequency-domain magnitude responses exist in each channel and zero time delay responses exist between the channels, it is apparent that the adaptive equalization process performed rather well. However, the overall system performance observable in the broadband sweep data still needs to be examined.

The broadband sweep data was taken utilizing the configuration depicted in Figure 29 and the procedures outlined in the uncompensated case. As in the uncompensated case, the noise source was swept horizontally across in front of the RUT as previously described in Section 3.1. Again, data was recorded at test point TP2 for both the in-phase and inverted cases.

After recording the data, time domain plots were generated for both cases, shown in Figures 32 and 33. Figure 32 is a plot of voltage versus time for a broadband sweep when both channels were driven in-phase. Notice the uniformity of the envelope in the center of the sweep. This is indicative of both channels being equalized reasonably well. If they were not, reduced levels would occur in the center of the sweep, as was shown in Figure 14. Figure 33 illustrates voltage versus time data for a broadband sweep when one channel was inverted from the other. Here, a null of approximately 19 dB is present in the center of the sweep, again pointing to good equalization. An uncompensated channel with very little level reduction is presented in Figure 15.

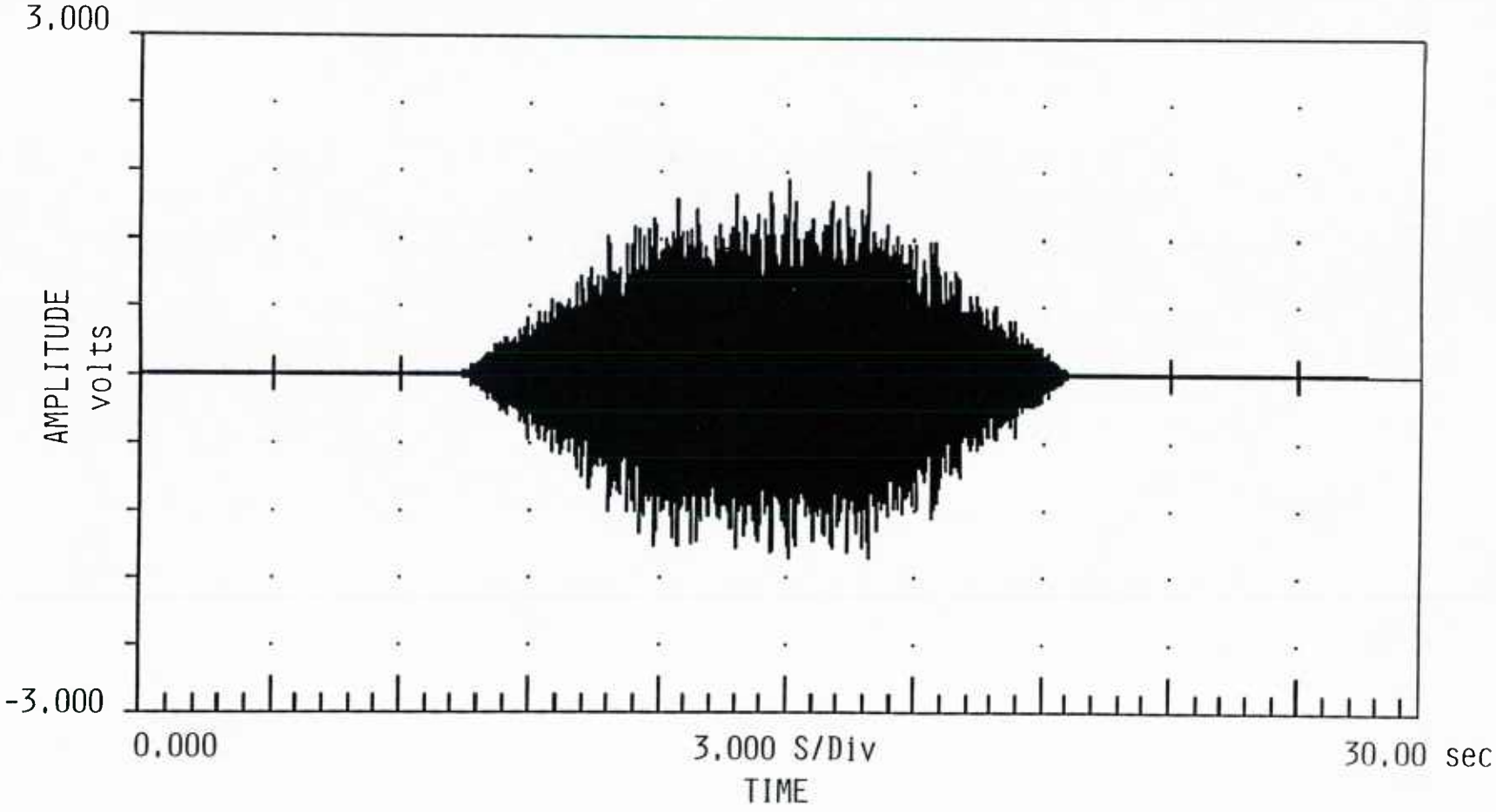

Figure 32. Voltage vs. Time Measured at TP2 for the Compensated In-phase Case

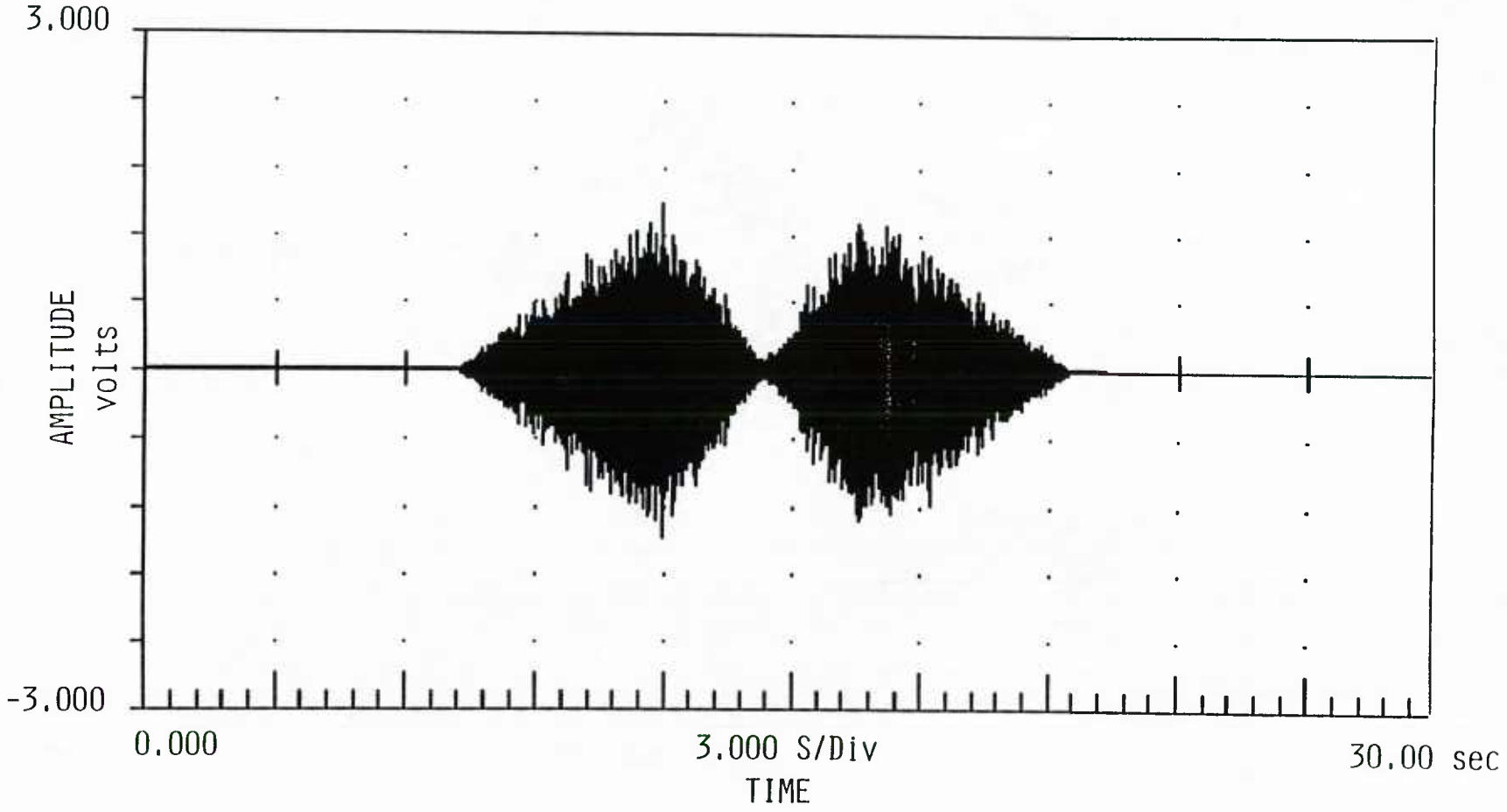

Figure 33. Voltage vs. Time Measured at TP2 for the Compensated Inverted Case

Chapter 4

COMPARISONS

The data from the compensation experiments was presented in Section 3.3, including observations during the compensation procedures as well as a description of channel performance after equalization. A comparison of channel performance before and after compensation will now be presented. Figures 34 through 39 provide illustrations characterizing each channel's magnitude response, time delay response, and overall system performance both before and after compensation.

Figures 34 and 35 show the magnitude responses before and after compensation for channels 1 and 2, respectively. In Figure 34, the compensated spectrum is uniform across the passband and is approximately 20 dB lower in magnitude than the uncompensated spectrum's peak amplitude. The 20 dB difference in channel gain is due to the equalizer, but it is of no consequence since it has already been established that the equalizer gain can be adjusted to the desired value. Furthermore, the 8 dB variation in magnitude across the passband in the uncompensated case, due primarily to the sin(x)/x operator, is eliminated by the equalizer. In Figure 35, it can again be seen that the characteristic sin(x)/x has been reduced to a uniform spectrum with reduced gain.

Figures 36 and 37 contain time delay information before and after compensation for channels 1 and 2, respectively. They are normalized cross-correlations between the delayed reference and the reference after it propagates through the channel. Note that the correlation peaks occur at nearly the same place when comparing compensated and uncompensated cases between the two figures. In addition, the time difference between

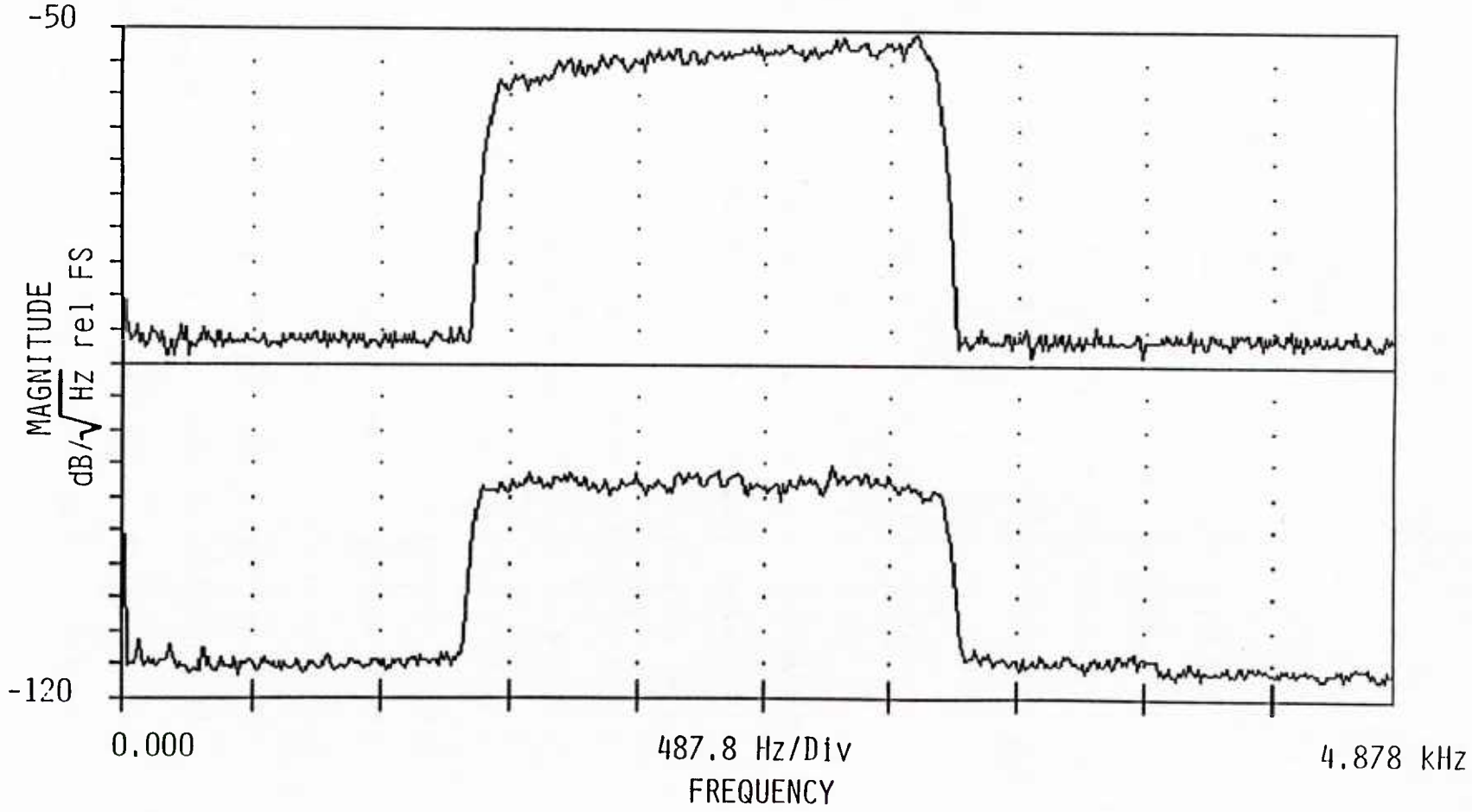

Figure 34. Power Spectral Density at TP2 When Channel 1 is Driven with the Broadband Noise Source of Figure 13 -- Top: Uncompensated, Bottom: Compensated

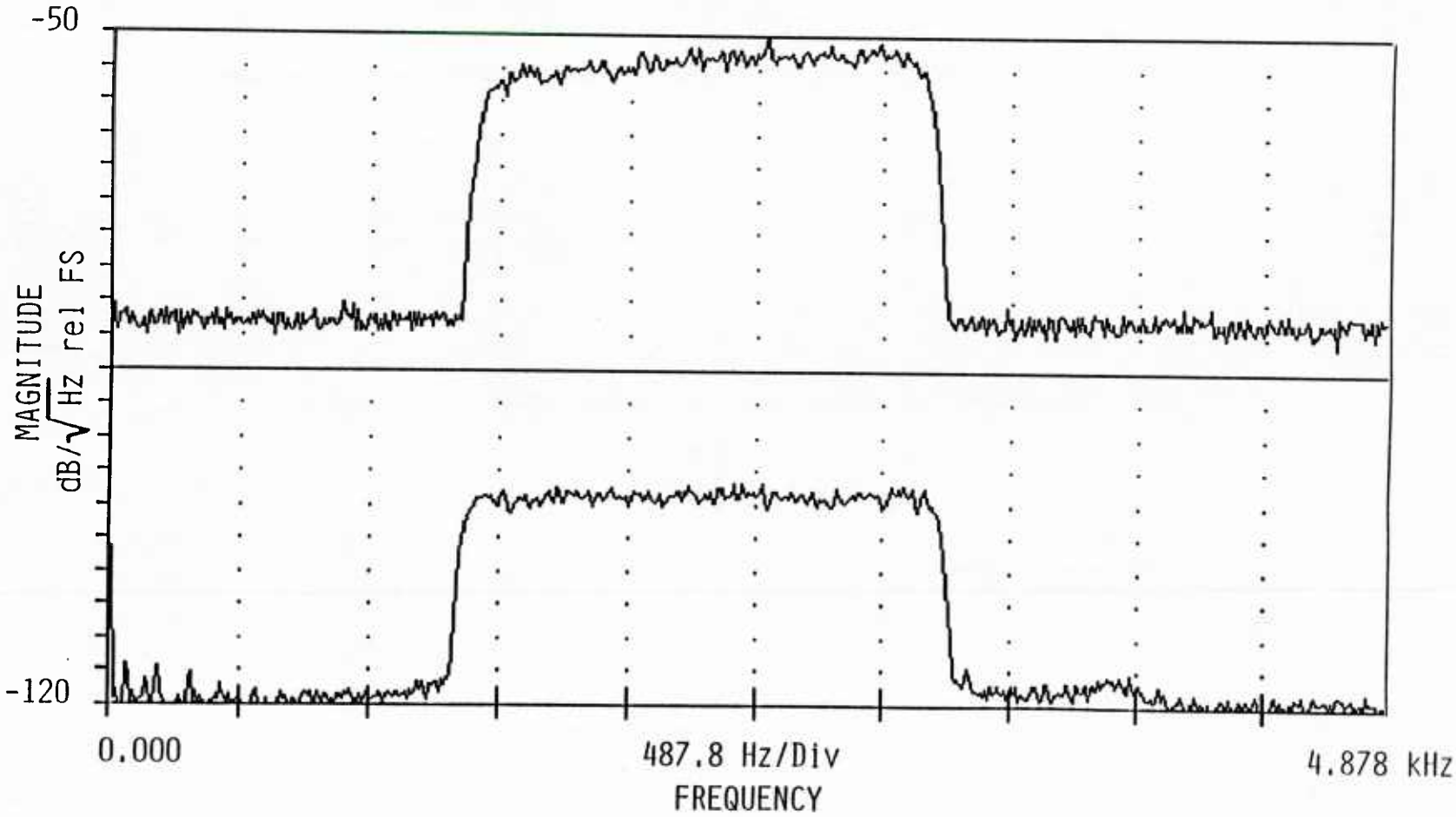

Figure 35. Power Spectral Density at TP2 When Channel 2 Is Driven with the Broadband Noise Source of Figure 13 -- Top: Uncompensated, Bottom: Compensated

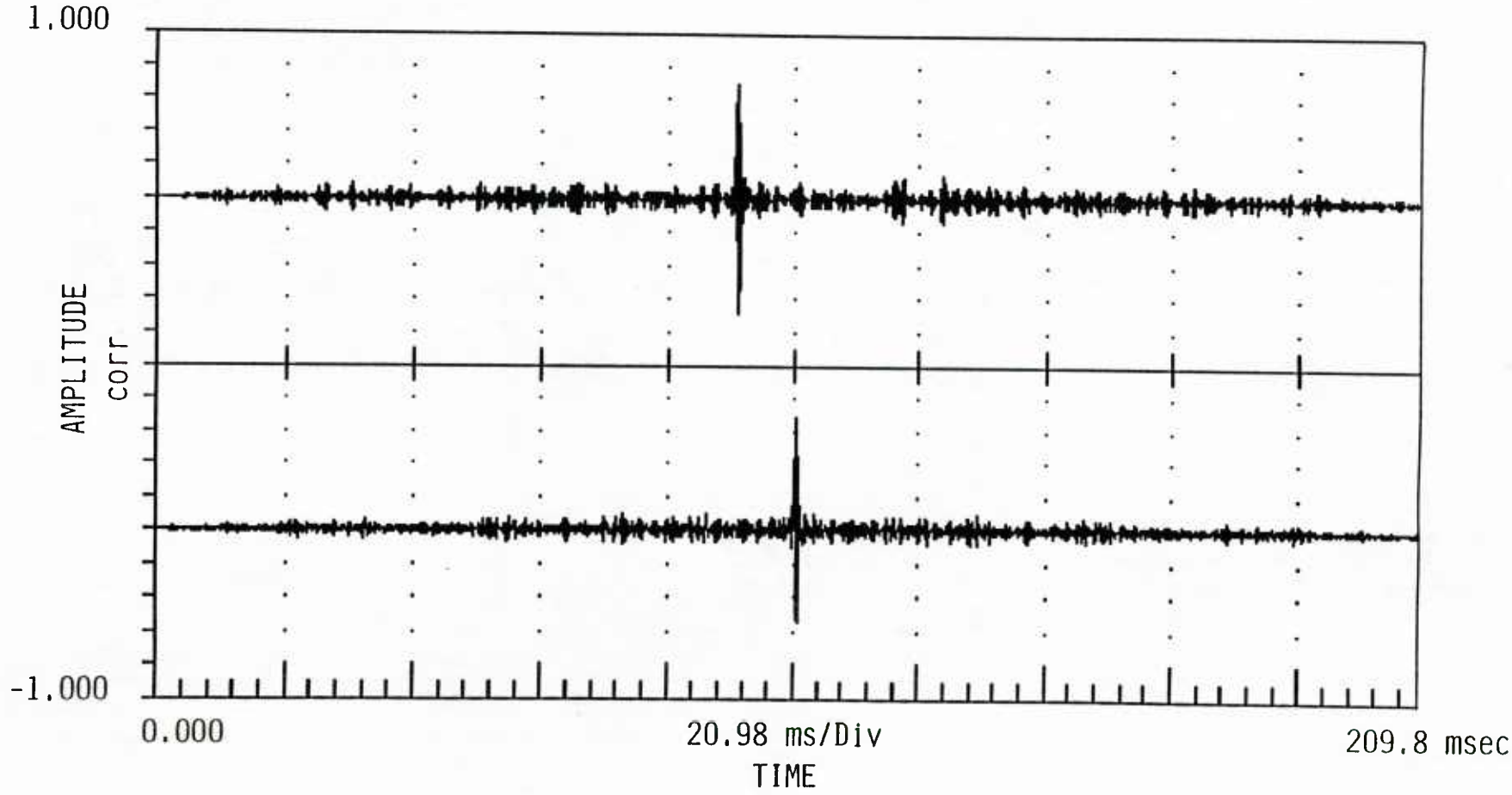

Figure 36. Normalized Cross-correlations for Channel 1 -- Top: Uncompensated Case, Bottom: Compensated Case

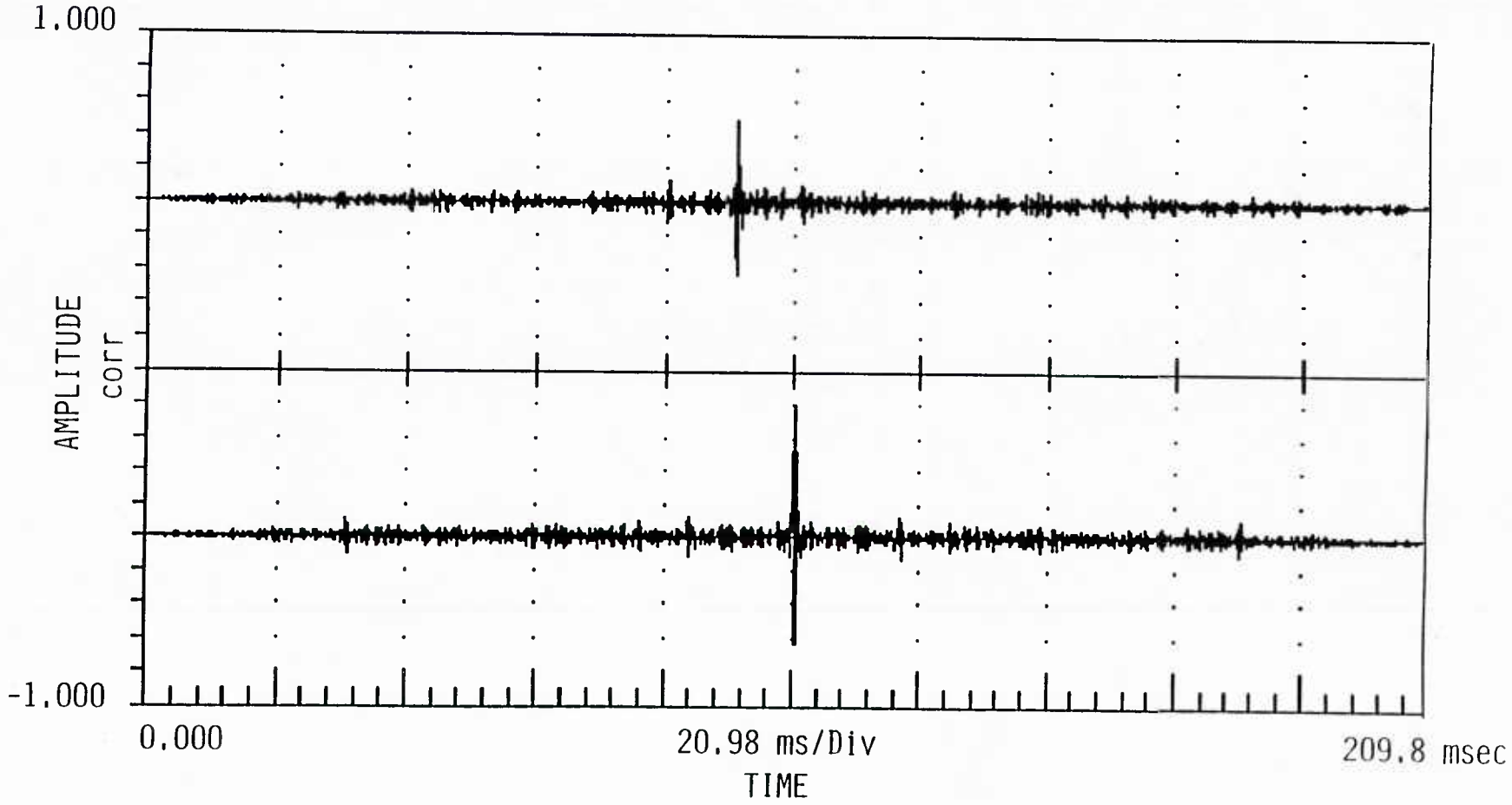

Figure 37. Normalized Cross-correlations for Channel 2 -- Top: Uncompensated Case, Bottom: Compensated Case

peaks when comparing the two cases within either Figure 36 or 37 is merely the equalizer filter delay, or 9.7 msec.

Finally, Figures 38 and 39 contain overall system performance information. These figures are amplitude versus time plots at the RUT when a broadband source was swept across in front of it. Figure 38 displays the data obtained when the two channels were driven 180 degrees out of phase. The top reflects the uncompensated data; the bottom demonstrates the effect of compensation, i.e., the desirable characteristic null due to the inverted signals. On the other hand, Figure 39 illustrates sweep data of the two channels driven in phase. Again, the uncompensated case is shown at the top while the compensated one is shown at the bottom. After compensation, the desirable uniform envelope is apparent in Figure 39 at the bottom.

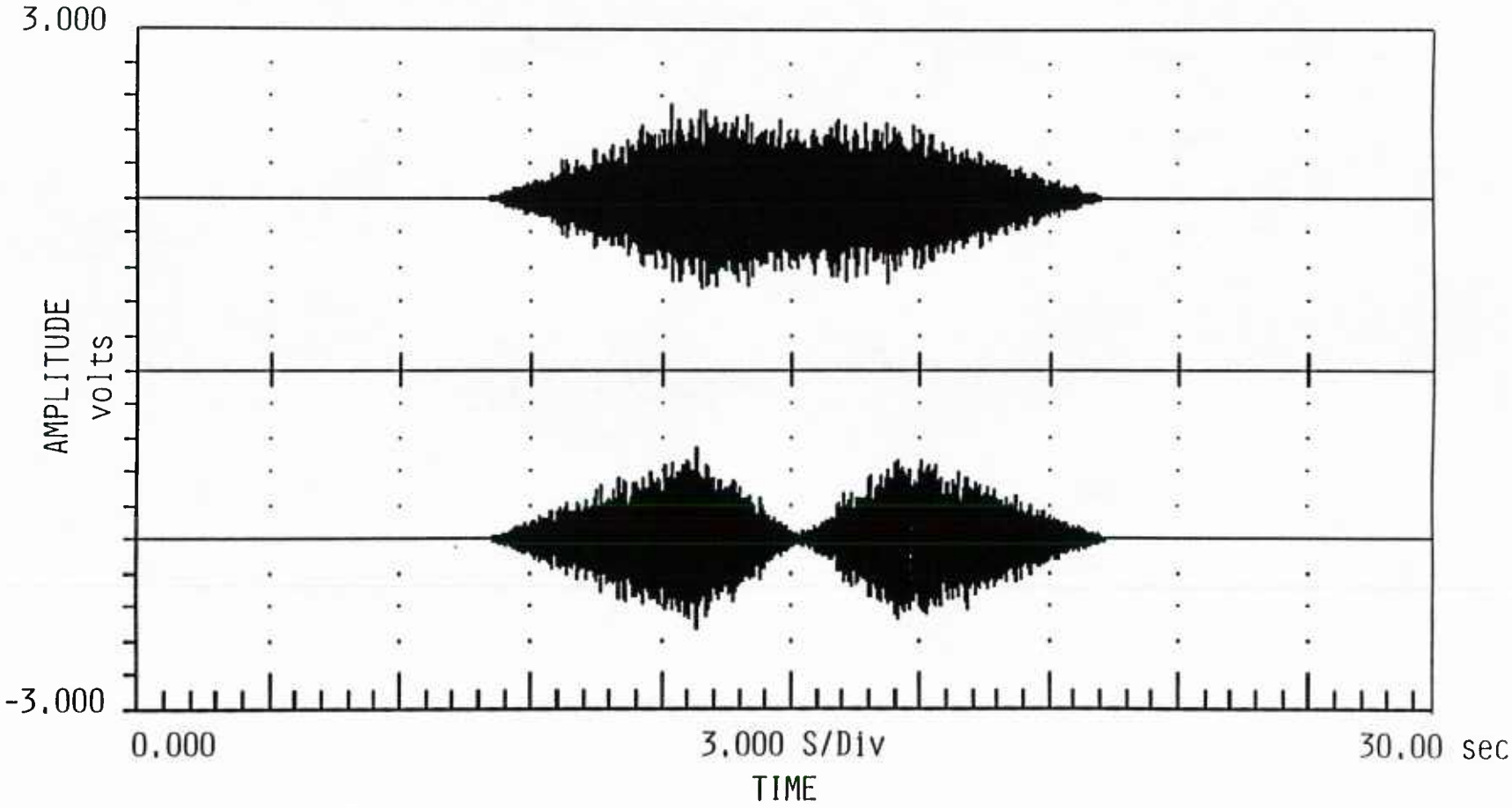

Figure 38. Voltage vs. Time at TP2 for a Broadband Sweep -- Top: Uncompensated Inverted, Bottom: Compensated Inverted

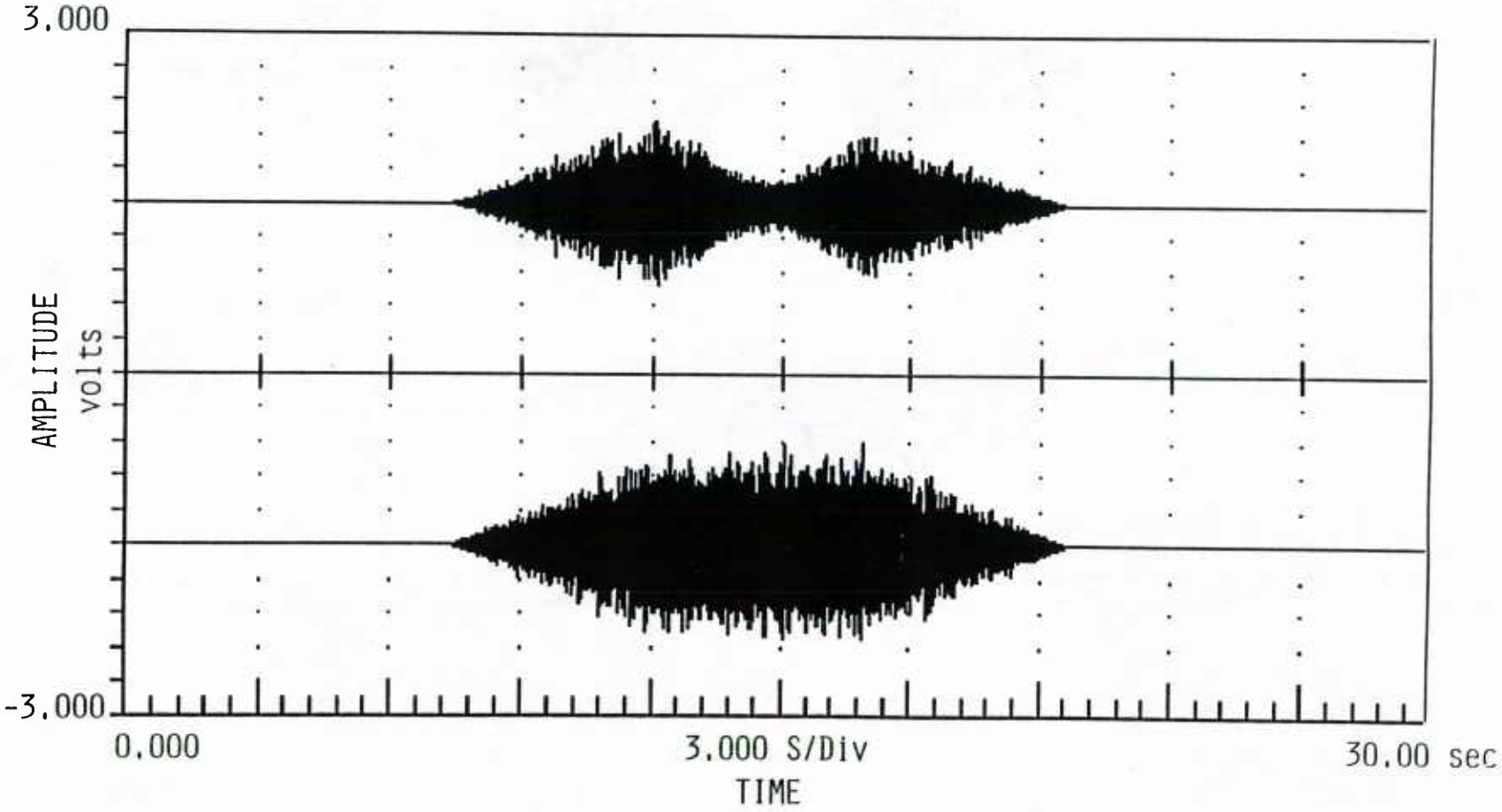

Figure 39. Voltage vs. Time at TP2 for a Broadband Sweep -- Top: Uncompensated In-phase, Bottom: Compensated In-phase

Chapter 5

SUMMARY AND CONCLUSION

Equalization is necessary in many instances where signal fidelity must be maintained throughout a channel's medium. The typical types of distortion responsible for a loss in signal fidelity are non-uniform time delay and non-uniform amplitude response in the frequency domain. A fixed network or transfer function can often be inserted in series with the channel path to correct the situation. However, in multiple-channel cases, repetitive filter alignment becomes a problem, and an adaptive equalization solution becomes more attractive. Automatic synthesis procedures allow path equalization in multiple-channel cases without information known a priori and without tedious alignment problems. Adaptive equalizers are most commonly used in communications to combat InserSymbol Interference (ISI). Of the different types of filter architectures and adaptive algorithms available, the most popular configuration is the transversal or FIR architecture used with the LMS algorithm of steepest descent.

Most of the research and literature concerning adaptive equalization revolves around the problem of ISI. The problem addressed in this publication is the multiple-channel equalization of a nearfield sonar system. The sonar system is a multiple-element, amplitude-shaded array that can project an acoustic field to a Receiver Under Test (RUT). Array shading enables the energy to be directed as though it came from some point in a subspace of three-dimensional space. The array's principle of operation requires that a coherent sum exist at the receiver's location when all array elements are being driven in phase. In order for this to occur, the effective acoustic path lengths of the channels must be equal. However, ensuring equal lengths is not a trivial problem due to the channels' electronics and the mechanical tolerances of the array's fixture.

Therefore, some form of equalization becomes necessary. Due to the multiplicity of the channels, an adaptive equalizer solution is desirable. The objective of the research and experimentation presented was to demonstrate an adaptive equalization scheme and its performance as a viable solution to the problem of multiple-channel equalization of a nearfield sonar system. To meet this objective and maintain simplicity, only two array elements in the horizontal plane were used.

Three experiments were performed to characterize each channel of the unequalized system. First, a broadband noise source was swept across in front of the array by properly shading each element in time synchronization. This was done once with both elements driven in phase and once with them driven 180 degrees out of phase. Ideal equalization results in a uniform envelope level for the in-phase case and a notched envelope for the out-of-phase case when measured at the RUT. However, experimental results show that the roles were almost reversed. The in-phase case presented somewhat of a notch at the center of the envelope, whereas the out-of-phase case provided a nearly uniform envelope.

In the second experiment, the same broadband noise was used to drive each channel independently while the other was inactive. FFTs performed on the data collected at the RUT then gave each channel's frequency-domain magnitude response. Each channel's response looked similar, with a strong sin(x)/x appearance contributed by the D/A converters of the power amplifiers driving the transducers.

Finally, the third experiment used the same data as in the second experiment. The input to the channel and RUT recordings were correlated with each other to produce a correlation peak at a time from which the channel delay could be extracted. The delay was 3.48 msec for channel 1, and the delay for channel 2 was 3.21 msec. This resulted in a delay difference of 270 μsec.

After unequalized characterization data was collected, the two channels were compensated, and the same three experiments conducted on the uncompensated channels were repeated. During these compensation experiments, data was collected which demonstrated adaptive filter convergence properties for each channel with loop gains of 0.5, 0.125, and 0.03125. Also, a set of data was obtained with a loop gain of 0.5 but with an input signal level decreased by 6 dB. In each case, the error signal envelope decayed exponentially but with various decay time constants. When the loop gain was 0.5, the time was 1.56 seconds, regardless of the 6 dB change in signal level. However, the last two loop gain settings (0.125 and 0.03125) resulted in times of 6.24 seconds and 23.76 seconds, respectively (increasing as expected for lower loop gains). Out of the four sets of weights extracted from the compensation procedures, the case with the 6 dB decreased signal level differed only in amplitude. An FFT taken of one set of weights shows the inverse sin(x)/x characteristic required to compensate for the sin(x)/x slope in the unequalized magnitude response data. When the in-phase and out-of-phase broadband sweeps were done with the channels equalized, the results approached the ideal case. A uniform envelope occurred for the in-phase case, while the out-of-phase case produced a distinct notch at the center of the envelope. As for the frequency-domain magnitude responses, the adaptive equalizer filter produced a composite response with a uniform gain across the passband of the system. Lastly, the filter responses added the correct time delays to each channel to produce a near-zero relative time delay between the two channels. This is necessary to provide a coherent sum at the RUT, a requirement for the amplitude-shaded array's principle of operation.

In conclusion, the purpose of this research and the ensuing experiments was to develop a solution to the problem of equalizing multiple channels of a nearfield sonar system. The main objective was to demonstrate an adaptive process and its ability to

provide a reasonable solution to the problem. First, system performance was illustrated before equalization. This indicated severe distortion was present and equalization was necessary to decrease the error in angular placement of acoustic energy. Each channel was then compensated, followed by an exhibit of the system's enhanced performance. Since the main objective was met, it can be concluded that this adaptive scheme provides a realizable and viable solution to the problem of multiple-channel equalization of a nearfield sonar system, the equalization being vitally important to the fundamental operation of the system.

REFERENCES

1. Ungerboeck, G., "Theory on the Speed of Convergence in Adaptive Equalizers for Digital Communication," *IBM Journal of Research and Development*, pp. 153-162, November 1972

2. Proakis, J. G., "Adaptive Digital Filters for Equalization of Telephone Channels," *IEEE Trans. on Audio and Electro Acoustics*, Vol. AU-18, No. 2, pp. 195-200, June 1970

3. Satorius, E. H. and Pack, J. D., "Application of Least Squares Lattice Algorithms to Adaptive Equalization," *IEEE Trans. on Communications*, Vol. COM-29, No. 2, pp. 89-95, February 1981

4. Lucky, R. W. and Rudin, H. R., "An Automatic Equalizer for General-Purpose Communication Channels," *The Bell System Technical Journal*, pp. 2179-2208, November 1967

5. Qureshi, S., "Adaptive Equalization," *IEEE Communications Magazine*, pp. 9-16, March 1982

6. Proakis, J. G., "Advances in Equalization for Intersymbol Interference," *Advances in Communication Systems*, pp. 123-198, 1975

7. Haykin, S., Introduction to Adaptive Filters, Macmillan Publishing Company, New York, pp. 159-160, 1984

8. Orfanidis, S. J., Optimum Signal Processing: An Introduction, 2nd Edition, Macmillan Publishing Company, New York, pp. 167-172, 404-428, 1988

9. Messerschmitt, D. G. and Honig, M. L., Adaptive Filters: Structures, Algorithms, and Applications, Kluwer Academic Publishers, Maryland, pp. 49-50, 1984

10. Widrow, B. and Stearns, S. D., Adaptive Signal Processing, Prentice-Hall Inc., New Jersey, pp. 66-89, 99-112, 232-250, 1985

11. Cascadable Adaptive Finite Impulse Response Digital Filter Chip, Motorola Inc., Arizona, pp. 1-13, 1987

12. Treichler, J. R. and Agee, B. G., "A New Approach to Multipath Correction of Constant Modulus Signals," *IEEE Trans. on Acoustics, Speech, and Signal Processing*, Vol. ASSP-31, No. 2, pp. 459-471, 1983

13. Proakis, J. G., Digital Communications, McGraw-Hill, 1989

14. Treichler, J. R., Johnson, C. R., and Larimore, M. G., Theory and Design of Adaptive Filters, Wiley, New York, 1987

15. Clark, A. P., Equalizers for Digital Modems, Halsted Press, New York, 1985

16. Widrow, B., McCool, J., and Ball, M., "The Complex LMS Algorithm," *Proc. IEEE*, Vol. 63, pp. 719-720, 1975

17. Oppenheim, A. V. and Schafer, R. W., Digital Signal Processing, Prentice-Hall, Englewood Cliffs, NJ, 1975

18. Satorius, E. H. and Alexander, S. T., "Channel Equalization Using Adaptive Lattice Algorithms," *IEEE Trans. on Communications*, Vol. COM-27, pp. 899-905, 1979

19. Cioffi, J. and Kailath, T., "Fast, Recursive Least-Squares, Transversal Filters for Adaptive Processing," *IEEE Trans. on Acoustics, Speech, Signal Processing*, Vol. ASSP-34, No. 304, 1984

20. Mueller, M. S., "Least-Squares Algorithms for Adaptive Equalizers," *Bell Syst. Tech. J.*, Vol. 60, pp. 1905-1925, 1981

21. Gitlin, R. D. and Magee, F. R., "Self-Orthogonalizing Adaptive Equalization Algorithms," *IEEE Trans. on Communications*, Vol. COM-25, No. 666, 1977

22. Chang, R. W., "A New Equalizer Structure for Fast Start-up Digital Communication," *Bell Syst. Tech. J.*, Vol. 50, pp. 1969-2014, 1971

23. McWhirter, J. G. and Shepherd, T. J., "Least-Squares Lattice Algorithm for Adaptive Channel Equalization -- A Simplified Derivation," *IEEE Proc.*, Vol. 130, Pt.F, No. 532, 1983

24. Bellanger, M. G., Adaptive Digital Filters and Signal Analysis, Marcel Dekker, New York, 1987

Appendix

EXPERIMENTAL SETUP AND PARTS LIST

Table A-1. Parts List of Components Used in Performing Experimental Measurements

ITEM	PART NUMBER	MANUFACTURER
1. Noise Generator	ARL106809	Applied Research Lab[1]
2. Power Amplifier	ARL99852	Applied Research Lab
3. Drive Element	ARL87870	Applied Research Lab
4. Hydrophone	F33	Naval Research Lab[2]
5. Receiver	ARL99847	Applied Research Lab
6. Adap. FIR	DSP56200	Motorola, Inc.[3]

(1) Applied Research Laboratory
The Pennsylvania State University
P. O. Box 30
State College, PA 16804

(2) Naval Research Laboratory
P. O. Box 568337
Orlando, FL 32856

(3) Motorola Semiconductor Products, Inc.
Box 20912
Phoenix, AZ 85036

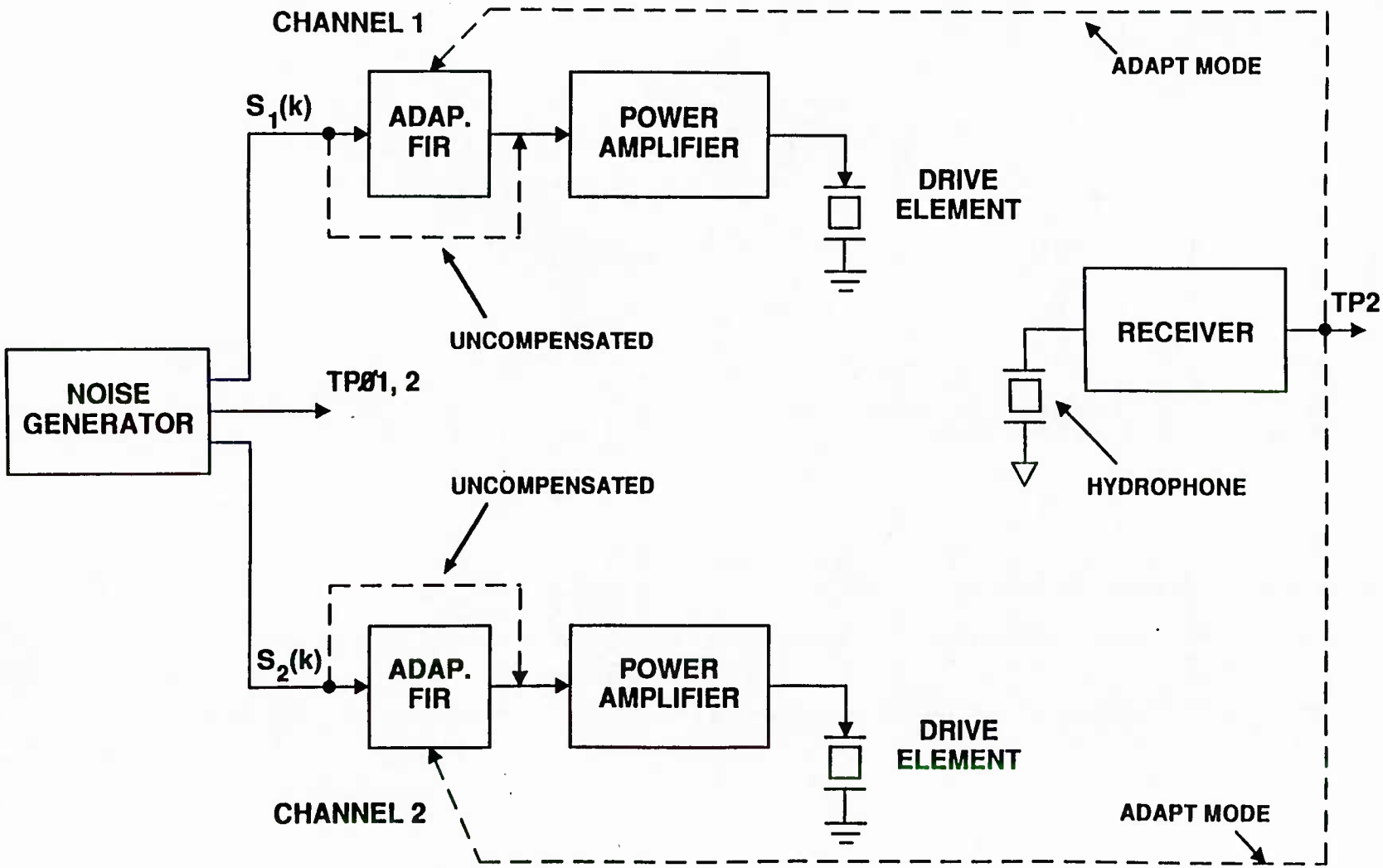

Figure A-1. Physical Setup Used In Performing Experimental Measurements

The Pennsylvania State University
Applied Research Laboratory
P.O. Box 30
State College, PA 16804